1   CYCLOPs: A Unified Framework for Surface Flux-Driven Cyclones Outside the Tropics

2   Kerry Emanuel (1), Tommaso Alberti (2), Stella Bourdin (3), Suzana J. Camargo (4,5), Davide
3   Faranda (6,7,8), Emmanouil Flaounas (9,10), Juan Jesus Gonzalez-Aleman (11), Chia-Ying Lee (4),
4   Mario Marcello Miglietta (12), Claudia Pasquero (13), Alice Portal (14), Hamish Ramsay (15), Marco
5   Reale (16), Romualdo Romero (17)

6   (1) Massachusetts Institute of Technology, 77 Mass. Ave., Cambridge, MA 02139

7   (2) Istituto Nazionale di Geofisica e Vulcanologia, Rome, Italy

8   (3) Atmospheric, Oceanic and Planetary Physics, Department of Physics, University of Oxford,
9   Oxford, United Kingdom

10   (4) Lamont-Doherty Earth Observatory, Columbia University, Palisades, New York, USA

11   (5) Columbia Climate School, Columbia University, New York, New York, USA

12   (6) Laboratoire des Sciences du Climat et de l'Environnement, UMR 8212 CEA-CNRS-UVSQ,
13   Université Paris-Saclay & IPSL, CE Saclay l'Orme des Merisiers, 91191 Gif-sur-Yvette,
14   France

15   (7) London Mathematical Laboratory, 8 Margravine Gardens, London W6 8RH, UK

16   (8) LMD/IPSL, ENS, Université PSL, École Polytechnique, Institut Polytechnique de Paris, Sorbonne
17   Université, CNRS, Paris France

18   (9) Institute for Atmospheric and Climate Science, ETH Zurich, Zurich, Switzerland

19   (10) Institute of Oceanography, Hellenic Centre for Marine Research, Athens, Greece

20   (11) Spanish State Meteorological Agency, AEMET, Department Development and Applications

21   (12) CNR-ISAC, Padua, Italy

22   (13) Department of Earth and Environmental Sciences, University of Milano - Bicocca, Italy

23   (14) Institute of Atmospheric Sciences and Climate (CNR-ISAC), National Research Council of Italy,
24   Bologna, Italy

25   (15) CSIRO Environment, Aspendale, Victoria, Australia

26   (16) National Institute of Oceanography and Applied Geophysics - OGS, Trieste, Italy

27   (17) Grup de Meteorologia, Departament de Física, Universitat de les Illes Balears, Palma de
28   Mallorca, Spain

29   Correspondence: Kerry Emanuel (emanuel@mit.edu)

30   Abstract

31   Cyclonic storms resembling tropical cyclones are sometimes observed well outside the
32   tropics. These include medicanes, polar lows, subtropical cyclones, Kona storms, and
33   possibly some cases of Australian East Coast Lows. Their structural similarity to tropical
34   cyclones lies in their tight, nearly axisymmetric inner cores, eyes, and spiral bands.
35   Previous studies of these phenomena suggest that they are partly and sometimes
36   wholly driven by surface enthalpy fluxes, as with tropical cyclones. Here we show,
37   through a series of case studies, that many of these non-tropical cyclones have
38   morphologies and structures that resemble each other and also closely match those of
39   tropical transitioning cyclones, with the important distinction that the potential intensity
40   that supports them is not present in the pre-storm environment but rather is locally
41   generated in the course of their development. We therefore propose to call these storms
42   CYClones from Locally Originating Potential intensity (CYCLOPs). We emphasize that
43   mature CYCLOPs are essentially the same as tropical cyclones but their development
44   requires substantial modification of their thermodynamic environment on short time
45   scales. Like their tropical cousins, the rapid development and strong winds of CYCLOPs
46   pose a significant threat and forecast challenge for islands and coastal regions, and the
47   effects of climate change on them should be considered.

48

49   # 1.   Introduction

50   Cyclones that resemble tropical cyclones are occasionally observed to develop well outside the
51   tropics. These include polar lows, medicanes, subtropical cyclones, Kona storms (central North
52   Pacific), and perhaps some cases of Australian East Coast Lows. The identification of such
53   systems is usually based on their appearance in satellite imagery and on the environmental
54   conditions in which they occur. Here we show that many of these systems are manifestations of
55   the same physical phenomenon and, as such, should be given a common, physically-based
56   designation. We propose to call these CYClones from Locally Originating Potential intensity
57   (CYCLOPs), with reference to the one-eyed creatures of Greek mythology[1]. We show that in
58   many respects these developments resemble classical "tropical transition" (TT) events (e.g.
59   Bosart and Bartlo, 1991), but they are distinguished from the latter by occurring in regions
60   where the climatological potential intensity is small or zero. (Some events previously identified
61   as TT events were probably examples of CYCLOPs.) Their often-rapid development and
62   intense mesoscale inner cores, compared to extratropical cyclones, make CYCLOPs significant
63   hazards and a forecasting challenge.

---

[1] Late in the process of writing this paper, we discovered that there is a scientific research project by the same name, standing for "Improving Mediterranean CYCLOnes Predictions in Seasonal forecasts with artificial intelligence" (https://www.cmcc.it/projects/CYCLOPs-improving-mediterranean-cyclones-predictions-in-seasonal-forecasts-with-artificial-intelligence). Its team leader, Leone Cavicchia, has graciously agreed with our use of the same name.

64   Cyclones of synoptic and sub-synoptic scale are powered by one or both of two energy sources:
65   the available potential energy (APE) associated with isobaric temperature gradients
66   (baroclinity), and fluxes of enthalpy (sensible and latent heat) from the surface (usually the
67   ocean) to the atmosphere[2]. A normal extratropical cyclone over land is an example of the
68   former, while the latter is epitomized by a classical tropical cyclone. Extratropical transitioning
69   and tropical transitioning cyclones[3] can be powered by both sources, either in sequence or with
70   the relative proportion varying over the life of the storm (see, e.g., Fantini, 1990). Additionally,
71   we note that tropical cyclones often originate in disturbances, such as African easterly waves,
72   that derive their energy from baroclinic and barotropic sources.

73   Like tropical cyclones, CYCLOPs are mainly powered by surface enthalpy fluxes, but differ from
74   the former in that the required potential intensity is produced locally and transiently, whereas
75   tropical cyclones develop in seasons and regions where sufficient potential intensity is always
76   present. CYCLOPs closely resemble the strongly baroclinic cases of tropical transition defined
77   and discussed by Davis and Bosart (2004), except that they occur in regions where the
78   climatological potential intensity is too small for tropical cyclogenesis, relying on synoptic-scale
79   perturbations that locally enhance potential intensity in space and time. Davis and Bosart (2004)
80   confined their attention to tropical cyclone formation in regions of high sea surface temperature,
81   stating that "The precursor cyclone must occlude and remain over warm water (≳26°C) for at
82   least a day following occlusion." Similarly, McTaggart-Cowan et al. (2008) and McTaggart-
83   Cowan et al. (2013) only examined cases of tropical transition that resulted in named tropical
84   cyclones. But McTaggert-Cowan et al. (2015) recognized that around 5% of the cases they
85   identified as tropical transition cases occurred over colder water and that upper-level troughs
86   played a key role in destabilizing the atmosphere with respect to the sea surface. We here build
87   on this work and place it within the framework of potential intensity theory.

88   The basic physics of CYCLOPs was explored by the first author in reference to medicanes
89   (Emanuel, 2005), and is illustrated in Figure 1. While the actual evolution is, of course,
90   continuous, it is simpler to discuss it in phases. For this narrow purpose, we assume that a cut-
91   off cyclone has already formed in the upper troposphere, signified by the presence of an
92   isolated potential vorticity (PV) anomaly near the tropopause (Figure 1a). We show an idealized
93   circularly symmetric anomaly and a cross-section through it; in practice, such developments are

---

[2] Some would regard latent heating as an additional energy source, but condensation through a deep layer is present in most cyclones and, being strongly tied to vertical motion, and one could argue that it should not be regarded as an external heat source but rather as a modification of the static stability (Emanuel et al., 1994). On the other hand, large areas of cyclones are not water saturated and various processes affect the availability of moisture in such regions, and thus, ultimately, the amount of latent heat release (e.g. Winschall et al., 2014). Moreover, latent heat release, when it is strong enough, can lead to the phenomenon of diabatic Rossby waves (Boettcher and Wernli, 2013; Kohl and O'Gorman, 2022; Parker and Thorpe, 1995; Wernli et al., 2002) and here the partitioning between advection and latent heating is important.

[3] Extratropical transitioning cyclones are storms whose energy source is transitioning from surface fluxes to ambient baroclinity, while the energy source of tropical transitioning cyclones is moving in the opposite direction.

94   seldom close to axisymmetric in their earlier stages. In the illustration, the first phase is
95   assumed to occur over land, but that need not be the case in general.
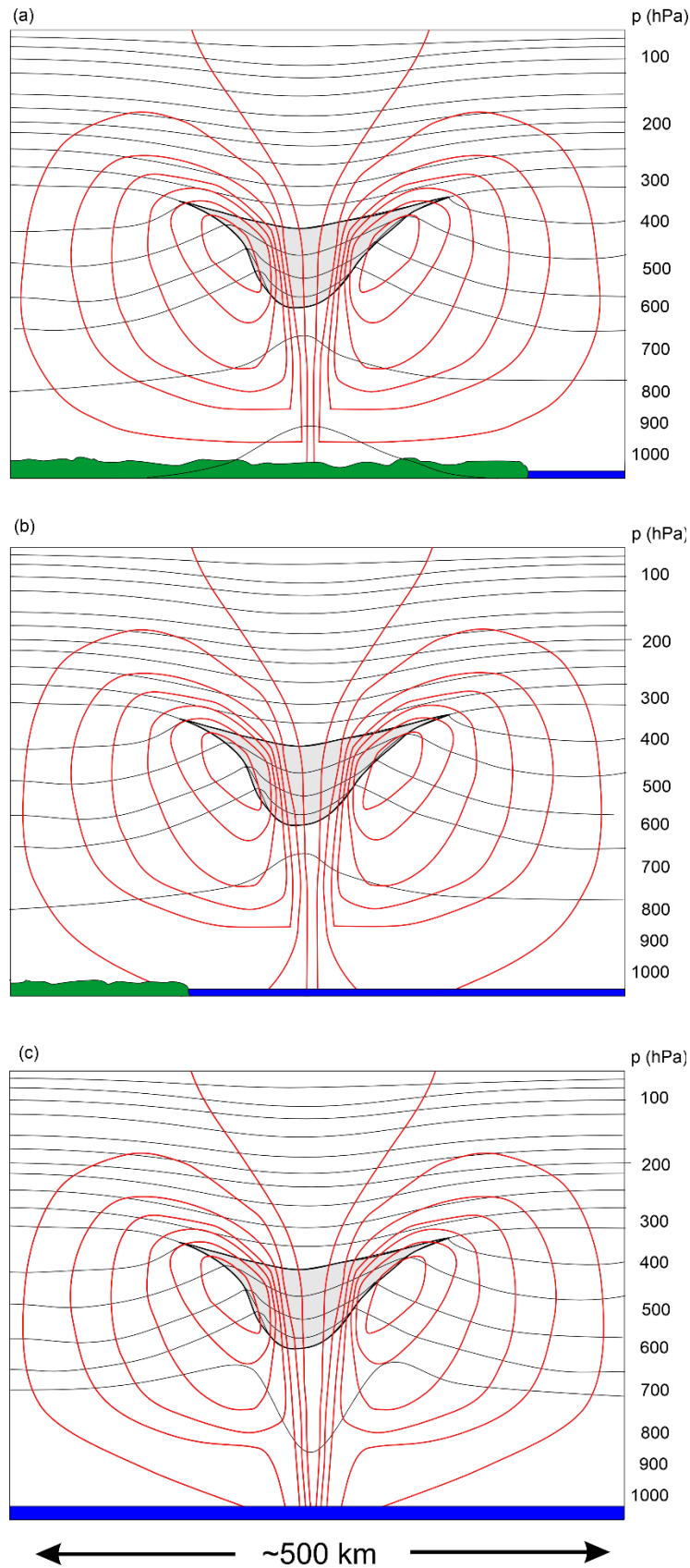
Figure 1: Three stages in the development of a CYCLOP. Each of the three panels shows a cross-section through an isolated PV anomaly at the tropopause (gray shading), idealized as circular. The thin black curves are isentropes, while the red curves are isotachs of the flow normal to the cross-section. In the first phase (a), the PV anomaly is over land, the troposphere beneath it is anomalously cold, and there may be no flow at the surface. The system moves out over open water in the next phase (b) and warming of the boundary layer and lower troposphere suffices to eliminate the cold anomaly at and near the surface. Weak cyclonic flow develops in response to the positive PV anomaly aloft. In the final phase (c), the surface heat fluxes become important and a tight, inner warm core develops.

~500 km

97   During the creation of the near-tropopause PV anomaly, some combination of lifting and cold air
98   seclusion has cooled and humidified the column underneath the PV anomaly, and the cold
99   anomaly extends right to the surface. From a PV inversion perspective, the near-surface
100 anticyclone that results from inverting the negative potential temperature anomaly at the surface
101 is assumed to just cancel the cyclonic anomaly that results from inverting the tropopause PV
102 anomaly, yielding no circulation at the surface. This assumption is made for simplicity here and
103 we do not mean to imply that such a cancellation is common.

104 In phase 2 (Figure 1b), the system drifts out over open water that is warm enough to diminish
105 and eventually eliminate the cold anomaly at the surface, "unshielding" it from the PV anomaly
106 aloft. During this phase, a cyclonic circulation develops in the lower troposphere, with a
107 horizontal scale commensurate with that of the PV anomaly.

108 If the local potential intensity is large enough, and the air aloft sufficiently close to saturation,
109 Wind-Induced Surface Heat Exchange (WISHE) can develop a tropical cyclone-like vortex
110 (phase 3, Figure 1c), with a warm inner core, eye and eyewall, and perhaps spiral bands. Note
111 that the inner core may be warm only with respect to the synoptic-scale cold anomaly
112 surrounding it, not necessarily with respect to the distant environment. At mid-levels, the
113 temperature anomaly may manifest as a small-scale warm anomaly surrounded by a synoptic-
114 scale cold anomaly.

115 In reality, these phases blend together into a continuum. Moreover, all three phases may (and
116 often do) occur over water. One practical challenge is calculating the potential intensity. This
117 should be calculated using the temperatures of the sea surface and the free troposphere under
118 the PV anomaly aloft, but before the troposphere has appreciably warmed from surface fluxes.
119 In practice, because the warming occurs either as the PV anomaly develops over water, or as it
120 moves over water from land, we have no access to the sounding of the free troposphere *before*
121 it has warmed up. The true potential intensity for a TC developing within the cold column under
122 the PV anomaly is hence impossible to obtain. Nevertheless, we can estimate how cold the
123 troposphere was before surface fluxes warmed it by using the surface pressure perturbation as
124 a proxy for the CYCLOPs-induced warming, and assuming that the troposphere has an
125 approximately moist adiabatic temperature profile[4]. This is derived in the Appendix. The result
126 is a modified potential intensity, V_{pm}, given by

$$V_{pm}^2 = V_p^2 - \frac{C_k}{C_D} \frac{T_s}{T_{400}} \phi_{950}', \tag{1}$$

128 where V_p is the potential intensity calculated in the usual way (e.g. Bister and Emanuel, 2002)

129 from the local sea surface temperature and atmospheric sounding, ϕ_{950}' is the perturbation away

130 from climatology of the near-surface geopotential, which we here evaluate at 950 hPa, C_k and

---

[4] In regions of deep convection, lapse rates are usually observed to be close to moist adiabatic (Betts, 1986)

131   C_D are the surface exchange coefficients for enthalpy and drag, and T_s and T_{400} are the

132   absolute temperatures at the surface and 400 hPa. As explained in the Appendix, we

133   approximate the coefficient multiplying ϕ'_{950} in (1) by a constant value, 1.3, a reasonable estimate

134   of the mean value of the coefficient. Note that (1) is only valid in places where our assumption

135   that the lapse rate is moist adiabatic trough a deep layer is valid and deep moist convection

136   occurs. Also, in the early stages of development, the outflow level is likely to be lower and the

137   outflow temperature correspondingly higher, reducing the value of the coefficient multiplying ϕ'_{950}

138   in (1).

139   Beginning with an upper cold cyclone in an environment of otherwise zero potential intensity,

140   Emanuel (2005) simulated the development of a WISHE-driven cyclone using the axisymmetric,

141   nonhydrostatic hurricane model of Rotunno and Emanuel (1987). The cold, moist troposphere

142   under such an upper cyclone proves to be an ideal incubator of surface flux-driven cyclones

143   with characteristics nearly identical to those of tropical cyclones. One interesting facet of the

144   process is that the anomalous surface enthalpy flux destroys the parent upper cold low over a

145   period of a few days, through the action of deep convection. This in another way in which

146   CYCLOPs are distinguished from tropical cyclones, which tap spatially extensive regions of high

147   potential intensity.

2.   Why it matters

149   Why should we care whether a cyclone is driven by surface fluxes or baroclinity? From a

150   practical forecasting standpoint, the spatial distributions of weather hazards, like rain and wind,

151   can be very different, as can be the development time scales and fundamental predictability.

152   In classical baroclinic cyclones, the strongest winds are often found in frontal zones and can be

153   far from the cyclone center, while precipitation is usually heaviest in these frontal zones and in a

154   shield of slantwise ascent extending poleward from the surface cyclone. There is long

155   experience in forecasting baroclinic storms, and today's numerical weather prediction (NWP) of

156   these events has become quite accurate, even many days ahead. Importantly, baroclinic

157   cyclones are well resolved by today's NWP models. While baroclinic cyclones can intensify

158   rapidly, both the magnitude and timing of intensification are usually forecast accurately, and

159   uncertainties are well quantified by NWP ensembles (Leutbecher and Palmer, 2008).

160   By contrast, the physics of tropical cyclone intensification, involving a positive feedback between

161   surface winds and surface enthalpy fluxes, results in an intense, concentrated core with high

162   winds and heavy precipitation (which can be snow in the case of polar lows). The eyewalls of

163   surface flux-driven cyclones are strongly frontogenetical (Emanuel, 1997), further concentrating

164   wind and rain in an annulus of mesoscale dimensions. The intensity of surface flux-driven

165   cyclones can change very rapidly and often unpredictably, presenting a severe challenge to

166   forecasters. For example, Hurricane Otis of 2023 intensified from a tropical storm to a Category

167   5 hurricane in about 30 hours, devastating Acapulco, Mexico, with little warning from

168   forecasters. The small size of the core of high winds and heavy precipitation means that small

169   errors in the forecast position of the center of the storm can lead to large errors in local wind and

170 precipitation predictions. Surface flux-driven cyclones are too small to be well resolved by
171 today's global NWP models, and even if they were well resolved, fundamental predictability
172 studies show high levels of intrinsic unpredictability of rapid intensity changes (Zhang et al.,
173 2014).

174 The time and space scales of surface flux-driven cyclones are such that they couple strongly
175 with the ocean, producing near-inertial currents whose shear-driven turbulence mixes to the
176 surface generally (but not always) colder water from below the surface mixed layer. This has an
177 important (usually negative) feedback on the intensification of such cyclones. Accurate
178 numerical forecasting of surface flux-driven cyclones therefore requires an interactive ocean,
179 generally missing from today's NWP models because it is not very important for baroclinic
180 cyclones and because of the additional computational burden.

181 For these reasons, it matters (or should matter) to forecasters whether a particular development
182 is primarily driven by surface fluxes or by ambient baroclinity. The structural differences
183 described above are often detectable in satellite imagery; at the same time, such imagery is
184 sometimes misleading about the underlying physics. For example, classical baroclinic
185 development sometimes develops cloud-free eyes surrounded by convection through the warm
186 seclusion process, even over land, and yet may not have the intense annular concentration of
187 wind and rain characteristic of surface flux-driven cyclones (Tous and Romero, 2013).

188

3.   Case Studies

190 Armed with the conceptual CYCLOP model developed in Section 1 and modified potential
191 intensity given by (1), we now turn to case studies of the development of medicanes, polar lows,
192 a subtropical cyclone, and a Kona storm, showing that the dynamic and thermodynamic
193 pathways are similar. Specifically, each case developed after the formation of a deep, cold-core
194 cut-off cyclone in the upper troposphere that often resulted from a Rossby wave breaking event.
195 The lifting of the tropospheric air in response to the developing potential vorticity anomaly near
196 the tropopause created a deep, cold, and presumably humid column. The deep cold air over
197 bodies of relatively warmer water substantially elevates potential intensity, while its high relative
198 humidity discourages evaporatively driven convective downdrafts, which tamp down the needed
199 increase in boundary layer enthalpy. Low vertical wind shear near the core of the cutoff cyclone,
200 coupled with high potential intensity and humidity, provide an ideal embryo for tropical cyclone-
201 like development. The requirement for low vertical wind shear may prevent open troughs from
202 producing CYCLOPs, even if the potential intensity is elevated.

203 In what follows we focus on the cut-off cyclone evolution and the development of modified
204 potential intensity. In a particular case, we compare reanalysis column water vapor to that
205 estimated from satellite measurements. The differences between these are significant enough
206 to cast some doubt on the quality of reanalyzed water vapor associated with the small-scale
207 CYCLOP developments, thus we do not focus on water vapor even though it is known to be
208 important for intensification of tropical cyclones.

209   We also examined, but do not show here, several cases of Australian East Coast Lows
210 (Holland et al., 1987). Owing to the East Australian Current, the climatological potential intensity
211 is substantial off the southeast coast of Australia, and the CYCLOP developments we analyzed
212 behaved more like classical tropical transitions, with little or no role of the synoptic scale
213 dynamics in enhancing the existing potential intensity. We suspect that there may be other
214 cases in which the latter process was important, but did not conduct a search for such cases. It
215 is clear that in many of these cases surface heat fluxes were important in driving the cyclone
216 (Cavicchia et al., 2019). We also examined a small number of subtropical cyclones that
217 developed in the South Atlantic, but as with the Australian cases, they resembled classical
218 tropical transitions, though again we suspect there may be CYCLOP cases there as well.

219 As with tropical cyclones, there are variations on the theme of CYCLOPs, and we explore these
220 in the closing sections.

221 ### 3.1 Medicane Celeno of January, 1995

222 On average, 1.5 medicanes are observed annually in the Mediterranean (Cavicchia et al., 2014;
223 Nastos et al., 2018; Romero and Emanuel, 2013; Zhang et al., 2021) and, more rarely, similar
224 storms are observed over the Black Sea (Yarovaya et al., 2008). We begin with a system,
225 Medicane Celeno, that reached maturity on 16 January, 1995, shown in infrared satellite
226 imagery in Figure 2.

227
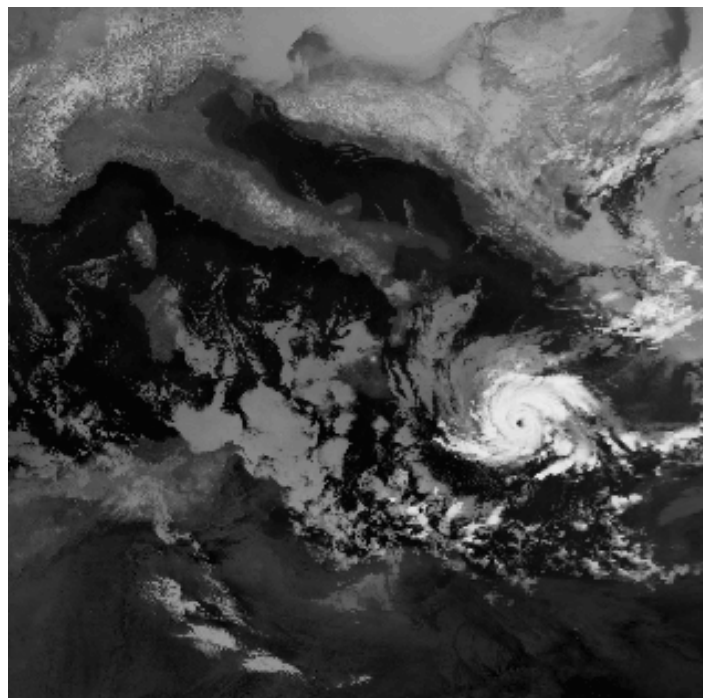
228   *Figure 2: Infrared satellite image of Medicane Celeno in the central Mediterranean, at 09:06 UTC 16 January 1995.*
229   *(Image credit: NOAA, 1995)*

230

231
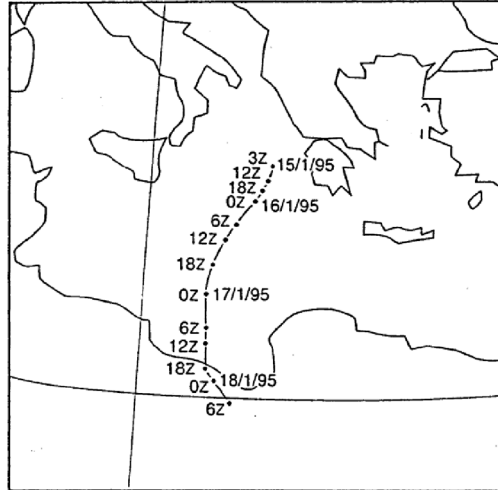
Figure 3: Track of the surface center of the cyclone between 03:00 UTC on January 15 and 06:00 on January 18, 1995, derived from satellite images (Pytharoulis et al.,1999)

Figure 3 shows the track of the surface center of the cyclone, which developed between Greece and Sicily and made landfall in Libya. A detailed description of this medicane is provided by Pytharoulis et al. (1999).

The evolution of the system in increments of 24 hours, beginning on 00 UTC, 12 January and ending at 00 UTC 15 January, is shown in Figure 4. This sequence, showing the 400 hPa and 950 hPa geopotential heights, covers the period leading up to the CYCLOP development. The evolution of the upper tropospheric (400 hPa) height field shows a classic Rossby wave breaking event (McIntyre and Palmer, 1983) in which an eastward-moving baroclinic Rossby wave at higher latitudes amplifies and irreversibly breaks to the south and west, finally forming a cut-off cyclone. It is important to note that the formation of a cut-off cyclone in the upper troposphere involves a local conversion from kinetic to potential energy, with deep cooling associated with dynamically forced ascent (Gan and Piva, 2016). To the southeast of this trough, a weak, broad area of low geopotential height develops at 950 hPa mostly over land in a region of low-level warm advection. As the cold air under the cut-off low is gradually heated by the underlying sea, a broad surface cyclone develops by 00 UTC on January 14th. At around this time, the feedback between surface wind and surface enthalpy fluxes is strong enough to develop a tight inner warm core (warm, that is, relative to the surrounding cold pool, not necessarily to the unperturbed larger scale environment) and by 00 UTC on January 15th, it is noticeable just to the west of northwestern Greece (Figure 5d). At the same time, the upper cold core weakens, perhaps aided by the strong heating from the surface transferred aloft by deep convection.
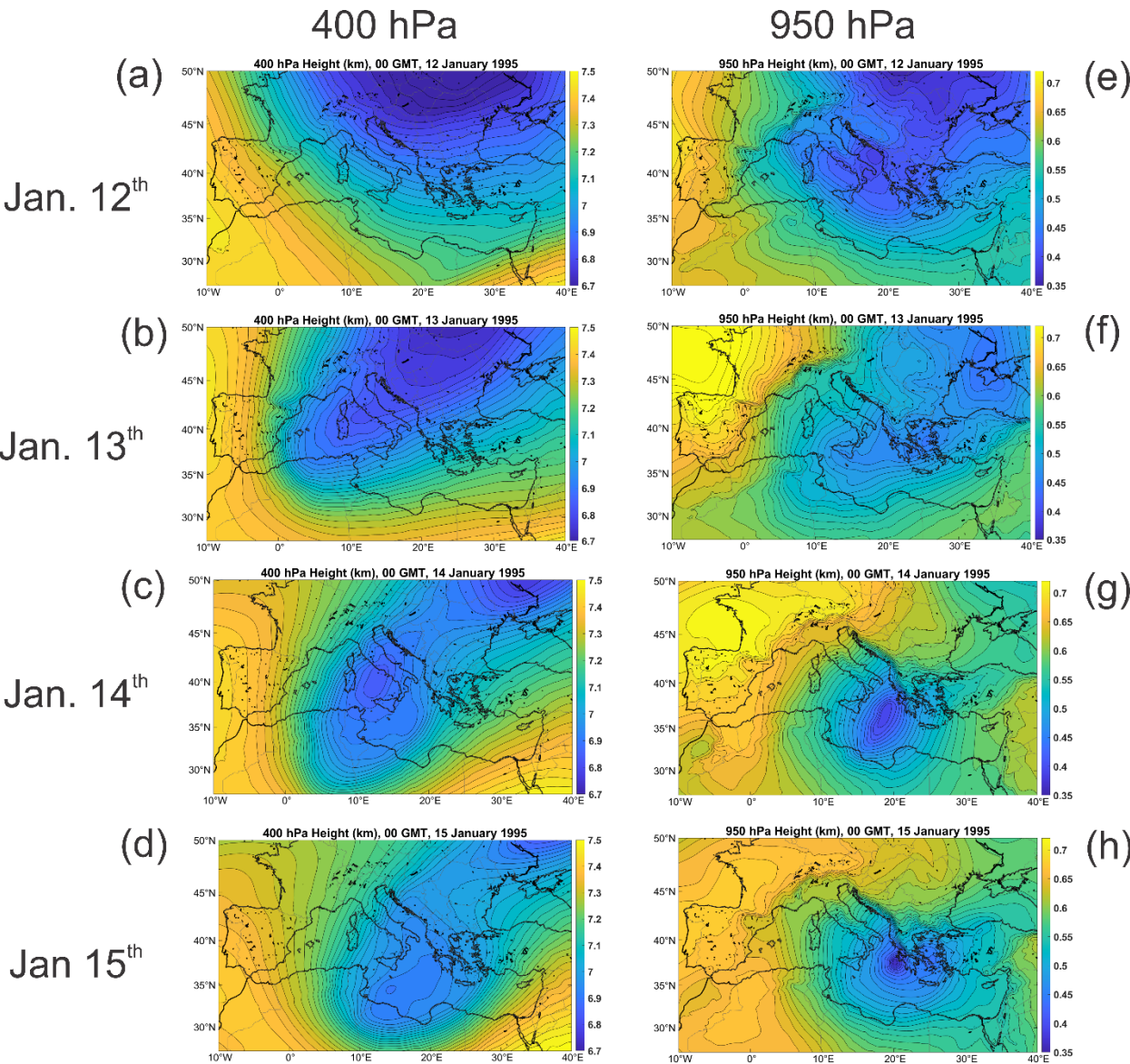
Figure 4: Evolution of the 400 hPa (left) and 950 hPa (right) geopotential heights in 24-hour increments, from 00 UTC 12 January to 00 UTC 15 January, 1995. These fields are from ERA5 reanalysis. The 400 hPa heights span from 6.7 to 7.5 km at increments of 26.67 m, while the 950 hPa heights range from 350 m to 730 m at increments of 12.67 m.

750 hPa T (K)   Modified Potential Intensity (m/s)

261
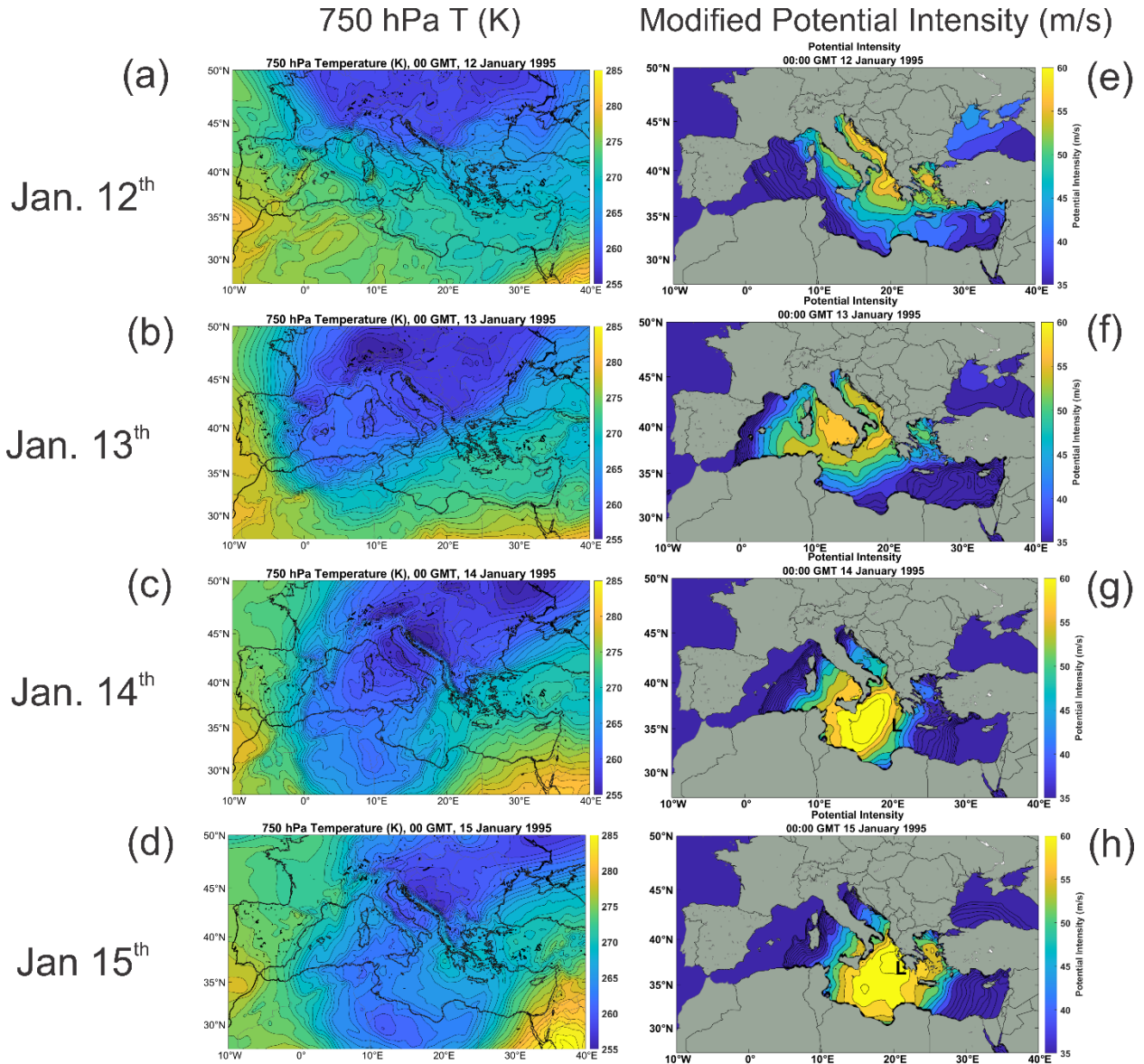
Figure 5: 750 hPa temperature (K; left) and modified potential intensity given by equation (1) (m/s, right) at 00 UTC on January 12th – 15th (top to bottom) 1995. The 750 hPa temperature spans from 255 K to 285 K at increments of 1 K, while the modified potential intensity ranges from 35 to 60 ms⁻¹ at increments of 4 ms⁻¹. The black "L"s in panels g) and h) show the positions of the surface cyclone. From ERA5 reanalysis.

266

267 Figure 5 shows the corresponding evolution of the 750 hPa temperature and the modified

268 potential intensity, V_{pm}, given by (1). The latter is only shown in the range of $35\ ms^{-1}$ to

269 $60\ ms^{-1}$. Experience shows that tropical cyclone genesis is rare when the potential intensity is

270 less than about $35\ ms^{-1}$ (Emanuel, 2010).

271   On January 12th, relatively small values of V_{pm} are evident in the eastern and northern

272   Mediterranean, but with higher values developing over the northern Adriatic as cold air aloft

273   creeps in from the north. As the upper tropospheric Rossby wave breaks and a cut-off cyclone

274   develops over the central Mediterranean, V_{pm} increases greatly during the 13th and 14th, with

275   peak values greater than $60\ ms^{-1}$. The CYCLOP develops in a region of high V_{pm}, though not

276   where the highest values occur, until the 15th at which time the mature CYCLOP location

277   corresponds to that of the highest V_{pm}. Note that a lower warm core is not obvious at 750 hPa

278   until January 15th and that it occurs on a somewhat smaller scale than the cut-off cyclone.

279   Figure A1 of the Appendix shows the individual contributions, on January 14th and 15th, of the

280   usual potential intensity (first term on the right side of (1)) and the correction for column warming

281   (second term on right of (1)) to the full potential intensity. (The contribution of column warming

282   was negligible before the 14th.) Note that the full potential intensity shown in Figure 5 *g* and *h* is

283   not the arithmetic sum of the two contributions but rather their Euclidean norm. The contribution

284   of the column warming, as measured by the surface pressure anomaly, is quite localized around

285   the CYCLOP and is located eastward of the maximum of the usual potential intensity.

286   As the CYCLOP moves southward, it maintains a tight inner warm core until after landfall (not

287   shown here) and the modified potential intensity, V_{pm}, over the south-central Mediterranean

288   diminishes rapidly, with peak values of only about $50\ ms^{-1}$ by 00 UTC on January 16th. One

289   potentially important difference between CYCLOP development and tropical transition is that in

290   the former case, the volume of air with appreciable potential intensity is limited. It is possible

291   that, by warming the whole tropospheric column relative to the surface, the enhanced surface

292   fluxes associated with the CYCLOP, acting through deep convection, substantially diminish the

293   magnitude and/or volume of the high V_{pm} air, serving to limit the lifetime of the CYCLOP. This

294   was the case in the axisymmetric numerical simulations of Emanuel (2005).

295   It is clear that this CYCLOP development occurred on time and space scales appreciably

296   smaller than those of the rather weak, synoptic-scale cyclogenesis resulting from the interaction

297   of the positive PV perturbation near the tropopause with a low-level temperature gradient. It is

298   also clear that the strong cooling of the troposphere in response to the development and

299   southward migration of the cutoff cyclone aloft was instrumental in bringing about the high

300   potential intensity necessary to activate the WISHE process. Therefore, the Rossby wave

301   breaking did much more than trigger cyclogenesis; it provided the necessary potential intensity

302   for the CYCLOP development. Here we draw a distinction from tropical transition, in which, in

303   most cases, the pre-existing potential intensity suffices to maintain a surface flux-driven cyclone.

304   We emphasize again that there is a gray area here consisting of flux-driven cyclones in which

305   the existing reservoir of potential intensity is enhanced to some degree by the local synoptic-

306   scale dynamics.

307

308   ## 3.2 Medicane of December 2005

309   A medicane, unofficially known as Zeo, formed on December 14th 2005 off the coast of Tunisia
310   and then moved eastward across a large stretch of the Mediterranean. Figure 6 shows a
311   satellite image of this medicane on December 15th. This cyclone has been the subject of
312   several intensive studies (e.g. Fita and Flaounas, 2018; Miglietta and Rotunno, 2019).

313
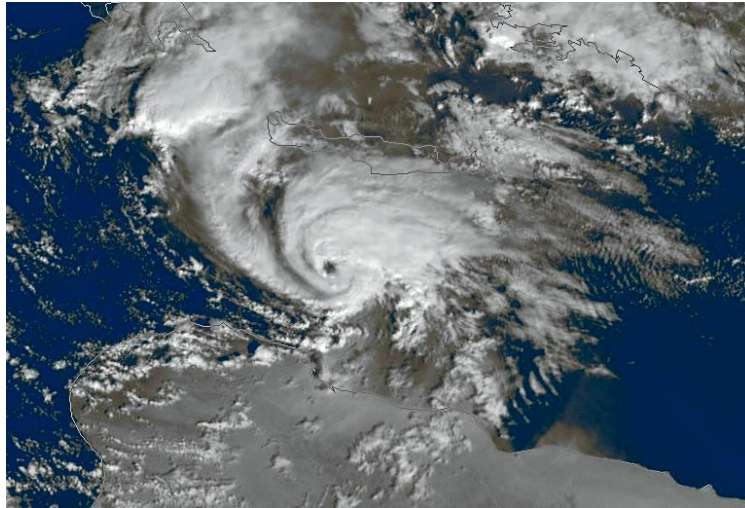
314   *Figure 6: Medicane Zeo between Crete and Libya on 15 December 2005. Image from NASA.*

315   Like Medicane Celeno, Medicane Zeo formed as a result of a Rossby wave breaking event, as
316   illustrated in Figure 7. On December 8th (panel a), a deep trough is digging southward over
317   eastern Europe, but by the 9th (panel b) it has split in two, with the westward half breaking
318   southwestward over Germany and Switzerland. By the 11th (panel d), this local minimum is
319   located over Tunisia and on the 12th (panel e) it is more or less completely cut off from the main
320   westerly jet. It subsequently oscillates over Tunisia and Algeria, before moving slowly eastward
321   over the Mediterranean, as shown in Figure 8.

322   In response to the cutoff cyclone development, a broad, synoptic-scale surface cyclone formed
323   to the east of the upper cyclone over the deserts of Libya during December 12th and 13th (not
324   shown here). The poorly defined center of this system drifted northward, on collision course with
325   the upper cyclone, which was drifting eastward over Tunisia by late on the 13th. As the surface
326   center moved out over the Mediterranean early on the 13th, rapid development ensued and a
327   mature CYCLOP was evident by 00 UTC on the 14th (Figure 8c). The system began to move
328   eastward and reached peak intensity on the 14th (left panels of Figure 8). The CYCLOP moved
329   eastward, along with its parent upper cyclone, and dissipated in the far eastern Mediterranean
330   on the 16th (not shown).

331

332

333
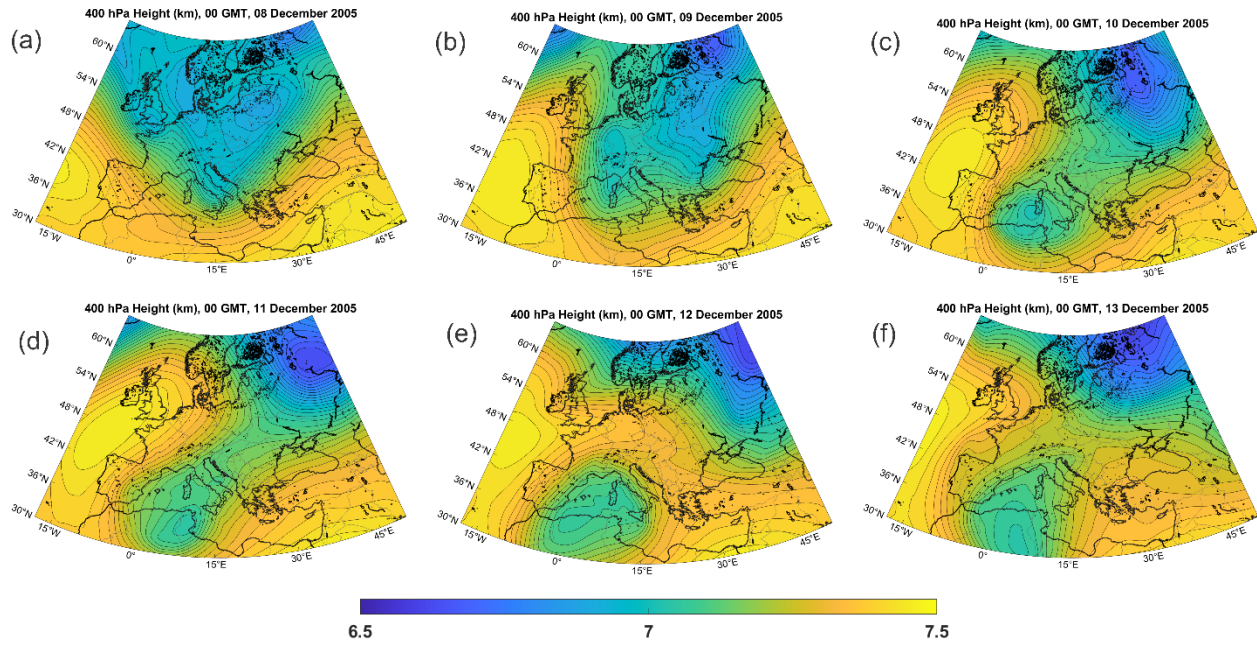
Figure 7: 400 hPa geopotential heights, ranging from 6.5 km to 7.5 km (color scale identical for all panels) at 00 UTC on December 8th (a), 9th (b), 10th (c), 11th (d), 12th (e), and 13th (f), 2005. From ERA-5 reanalysis. Contour interval is 33.3 m.

337   The evolutions of 750 hPa temperature and V_{pm} on the 14th and 15th of December are shown in

338   Figure 9. In this case, there were large meridional gradients of sea surface temperature across

339   the Mediterranean, ranging from over 20°C in the far south to less than 12°C in the northern

340   reaches of the Adriatic and western Mediterranean (not shown here). As the cold pool moved

341   southwestward and deepened, only low values of V_{pm} are present over the Mediterranean, but

342   beginning on December 10th, higher values developed over the Gulf of Sidra, east of Tunisia,

343   and by the 14th (Figure 9c) had reached at least 80 ms^{-1}, enabling the formation of the CYCLOP.

344   As in the Celeno case, V_{pm} values diminish thereafter, possibly because of the warming of the

345   column by the surface enthalpy flux.

346

347
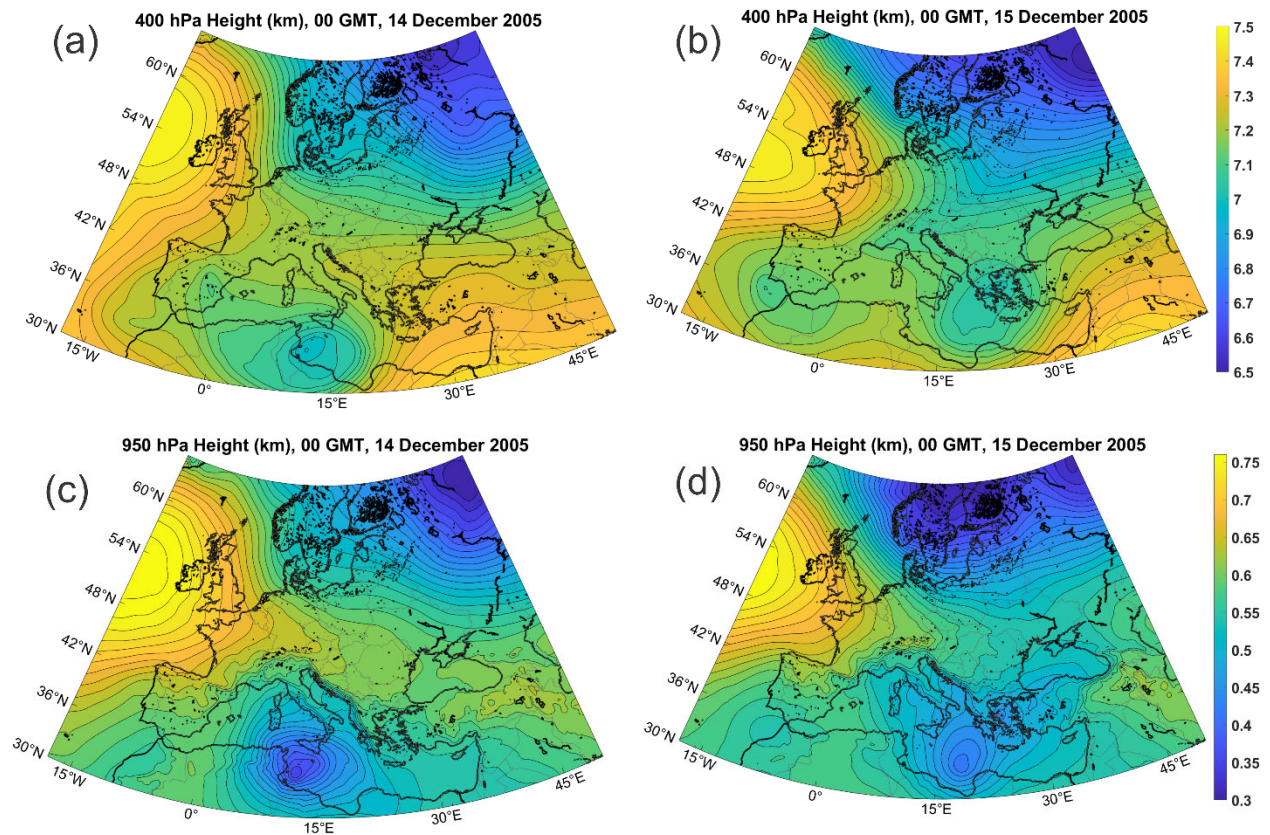
Figure 8: *Evolution of 400 hPa geopotential height, ranging from 6.5 to 7.5 km at contour interval of 36.7 m (a and b), and 950 hPa geopotential height, ranging from 250 to 750 m at contour interval of 16.67 m (c and d) at 00 UTC in December 14th (left) and 15th (right), 2005. The color scales of (a) and (b) are identical, as are the color scales of (c) and (d). From ERA-5 reanalysis.*

348
349
350
351

352

353

354

355
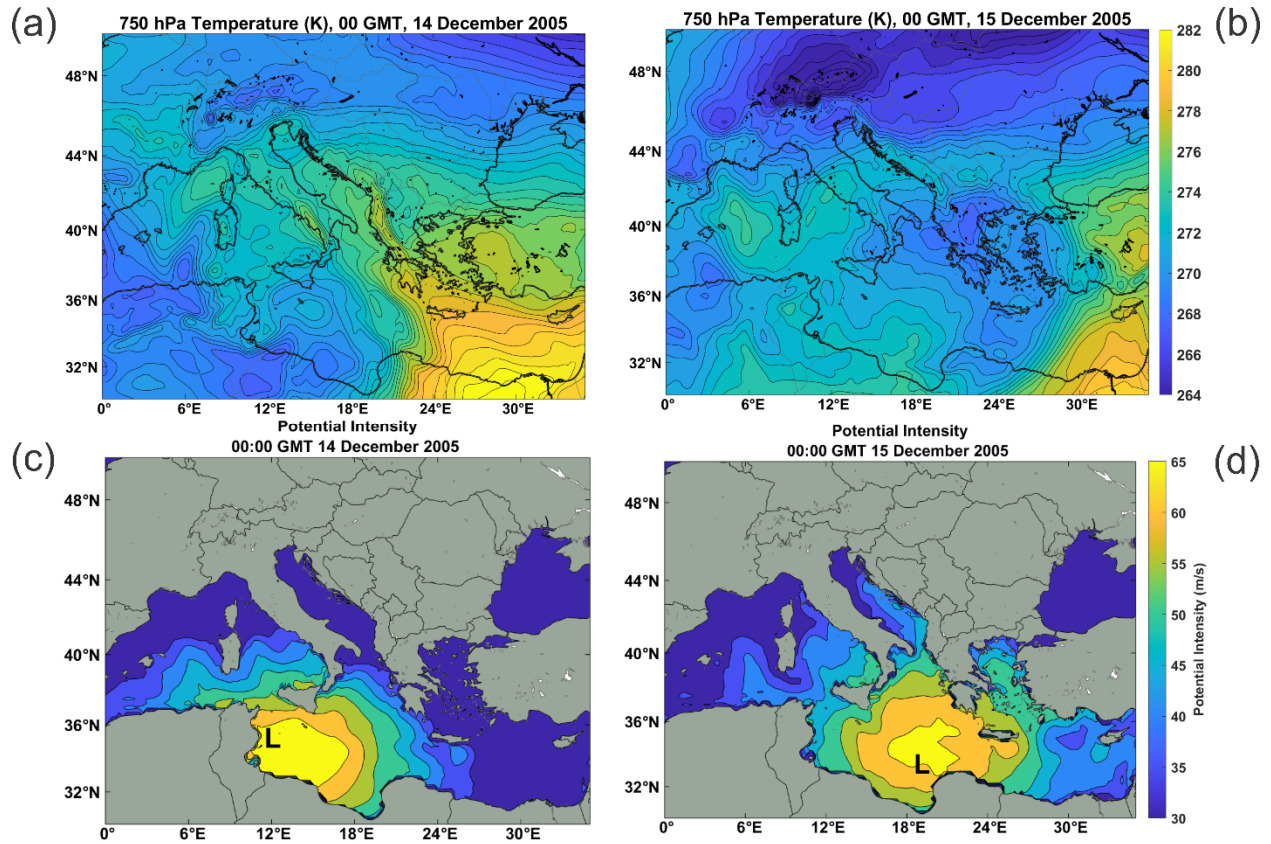
Figure 9: 750 hPa temperature at increments of 0.6 K (a-b) and modified potential intensity from 35 m s^{-1} to 65 m s^{-1} at increments of 5 m s^{-1} (c-d) at 00 UTC on December 14th (a,c) and December 15th (b,d) 2005. From ERA-5 reanalyses. The "L"s in c) and d) indicate the position of the 950 hPa cyclone center.

The 750 hPa temperature field (Figure 9a) shows a complex pattern of positive temperature perturbation near the position of the surface low, not nearly as focused as in the case of Medicane Celeno. As suggested by Fita and Flaounas (2018), part of the positive temperature anomaly associated with the cyclone may have resulted from a warm seclusion. Yet 24 hours later (Figure 9b) the warm anomaly near the cyclone center over the eastern Gulf of Sidra appears to have been advected from the south rather than the north. It is possible that the reanalysis did not capture the full physics of this particular medicane.

Figure 10 compares total column water retrieved from satellite microwave and near-infrared imagers (a) to that from the ERA5 reanalysis (b). While there is some broad agreement between the two estimates, the ERA5 underestimates column water in the critical region just east of Tunisia and overestimates it in an arc extending from eastern Sicily southeastward to the Libyan coast. Cyclop intensity, in analogy to tropical cyclone intensity, should be highly sensitive to low- and mid-level moisture in the mesoscale inner core region, which may be under-resolved and otherwise not well simulated by global NWP models. For this reason, we do not routinely show reanalysis of water vapor in this paper. The limitations of analyzed and forecast water vapor

374 may constitute an important constraint on CYCLOP predictability and is a worthy subject for
375 future research.
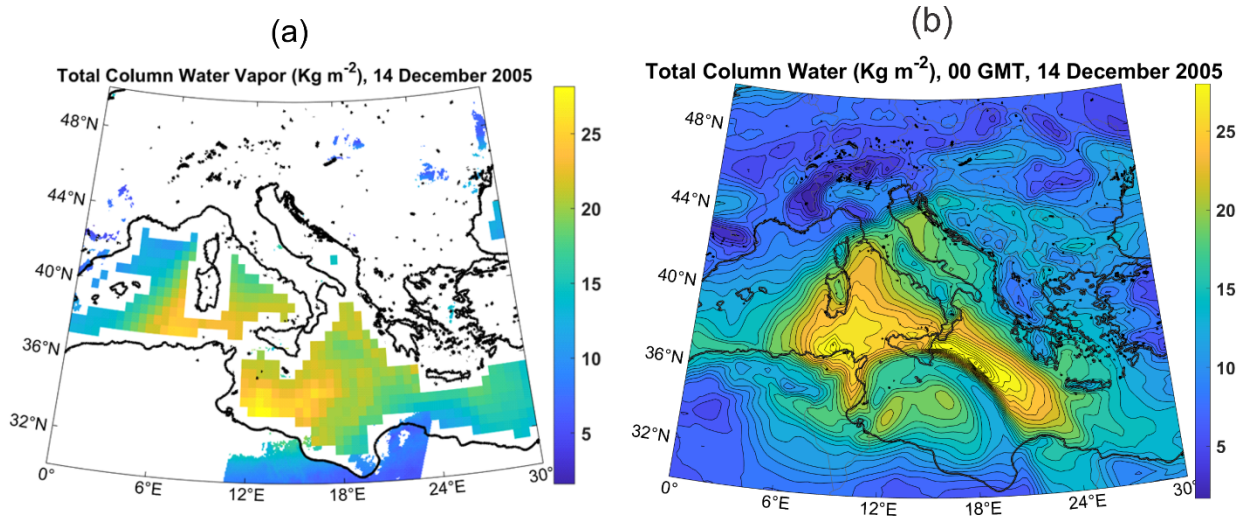
377 Figure 10: Total column water vapor (Kg m⁻²) at 00 UTC on 14 December 2005, derived from microwave and near
378 infrared imagers (a) and ERA5 reanalysis (b). In (b) the contour increment is 0.9 Kg m⁻².

3.3 Polar low of February, 1987

381 Closed upper tropospheric lows also provide favorable environments for CYCLOP development
382 at very high latitudes in locations where there is open water. These usually form poleward of the
383 mid-latitude jet, where quasi-balanced dynamics can be quite different from those operating at
384 lower latitudes. Figure 11 is an infrared image of a polar low that formed just south of Svalbard
385 on February 25th, 1987, and tracked southward, making landfall on the north coast of Norway on
386 the 27th. This system was studied extensively by Nordeng and Rasmussen (1992).

387
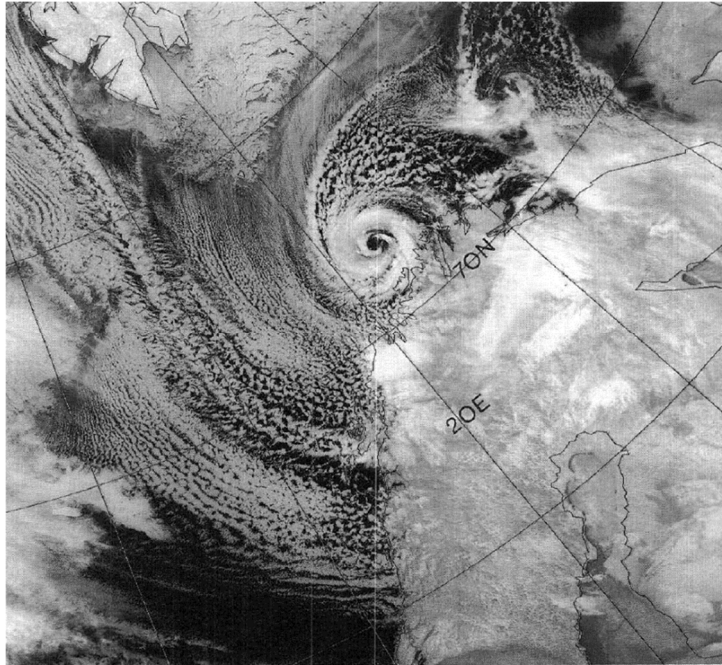
Figure 11: NOAA 9 satellite infrared image (channel 4) of a polar low just north of Norway at 08:31 UTC on 27 February 1987.

As with some medicanes, polar lows develop in strongly convecting air masses when cold air moves out over relatively warm water. The adjective "relatively" is crucial here; with polar lows the sea surface temperature is often only marginally above the freezing point of saltwater. Figure 12 shows the distribution of sea surface temperature on February 25th, with the uniform dark blue areas denoting regions of sea ice cover. The polar low shown in Figure 11 develops when deep cold air moves southward over open water, as shown in Figure 13.

In this case, it is not clear whether one can describe what happens in the upper troposphere (top row of Figure 13) as a Rossby wave breaking event. Instead, what we see is a complex rearrangement of the tropospheric winter polar vortex, as a ridge building over North America breaks and forms an anticyclone over the North Pole. This complex rearrangement results in the formation of a deep cutoff low just south of Svalbard by the 26th, which then moves southward over Norway by the 27th. The polar low is barely visible in the 950 hPa height field on the 25th (middle row of Figure 13), but intensifies rapidly as it moves over progressively warmer water, reaching maturity before landfall on the 27th.

404

405
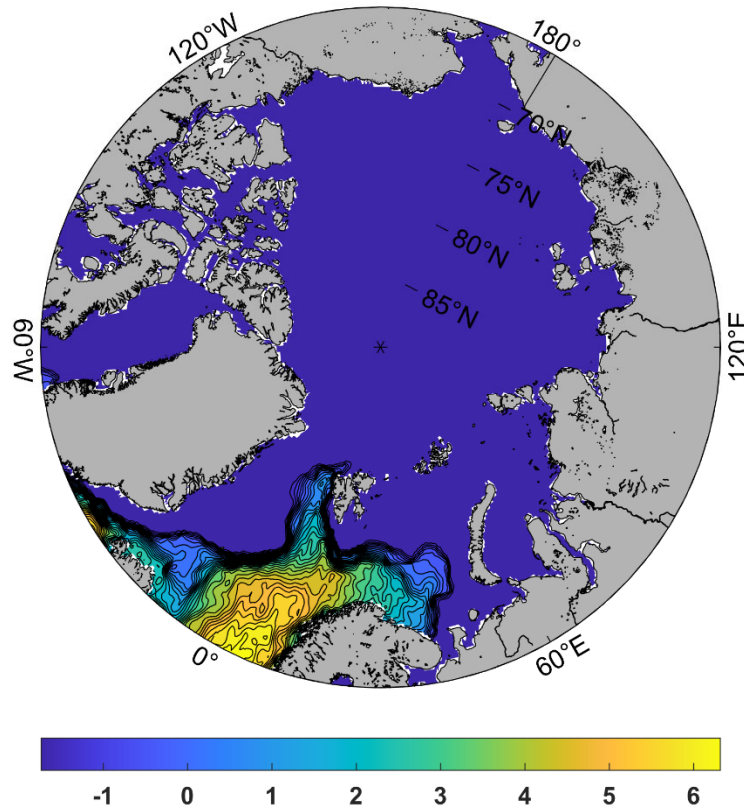
Figure 12: Sea surface temperature (ºC) in intervals of 0.3ºC at 02:00 UTC on 25 February, 1987, from ERA5
reanalysis. Dark blue areas denote regions of sea ice. From ERA-5 reanalyses.

408 The evolution of the V_{pm} field is shown in the bottom row of Figure 13. The potential intensity

409 increases rapidly south of Svalbard as the cut-off cyclone moves out over open water. ~~(The~~

410 ~~secondary region of high potential intensity, poleward of Siberia, is owing to relatively high ice~~

411 ~~surface temperature in a region covered with sea ice. As there is very little heat flux through sea~~

412 ~~ice, a CYCLOP cannot develop in this region, but a weak and broad surface low is associated~~

413 ~~with the cutoff cyclone in the upper troposphere.)~~

414 Under these conditions, most of the surface flux that drives the CYCLOP is in the form of

415 sensible, rather than latent heat flux, and the background state has a nearly dry (rather than

416 moist) adiabatic lapse rate. As shown by Cronin and Chavas (2019) and Velez-Pardo and

417 Cronin (2023), surface flux-driven cyclones can develop in perfectly dry convecting

418 environments, though they generally reach smaller fractions of their potential intensity and lack

419 the long tail of the radial profile of azimuthal winds that is a consequence of the dry stratification

420 resulting from background moist convection (Chavas and Emanuel, 2014). They also have

421 larger eyes relative to their overall diameters. Given the low temperatures at which they occur,

422 polar lows may be as close to the Cronin-Chavas dry limit as one might expect to see in Earth's

423 climate.

424
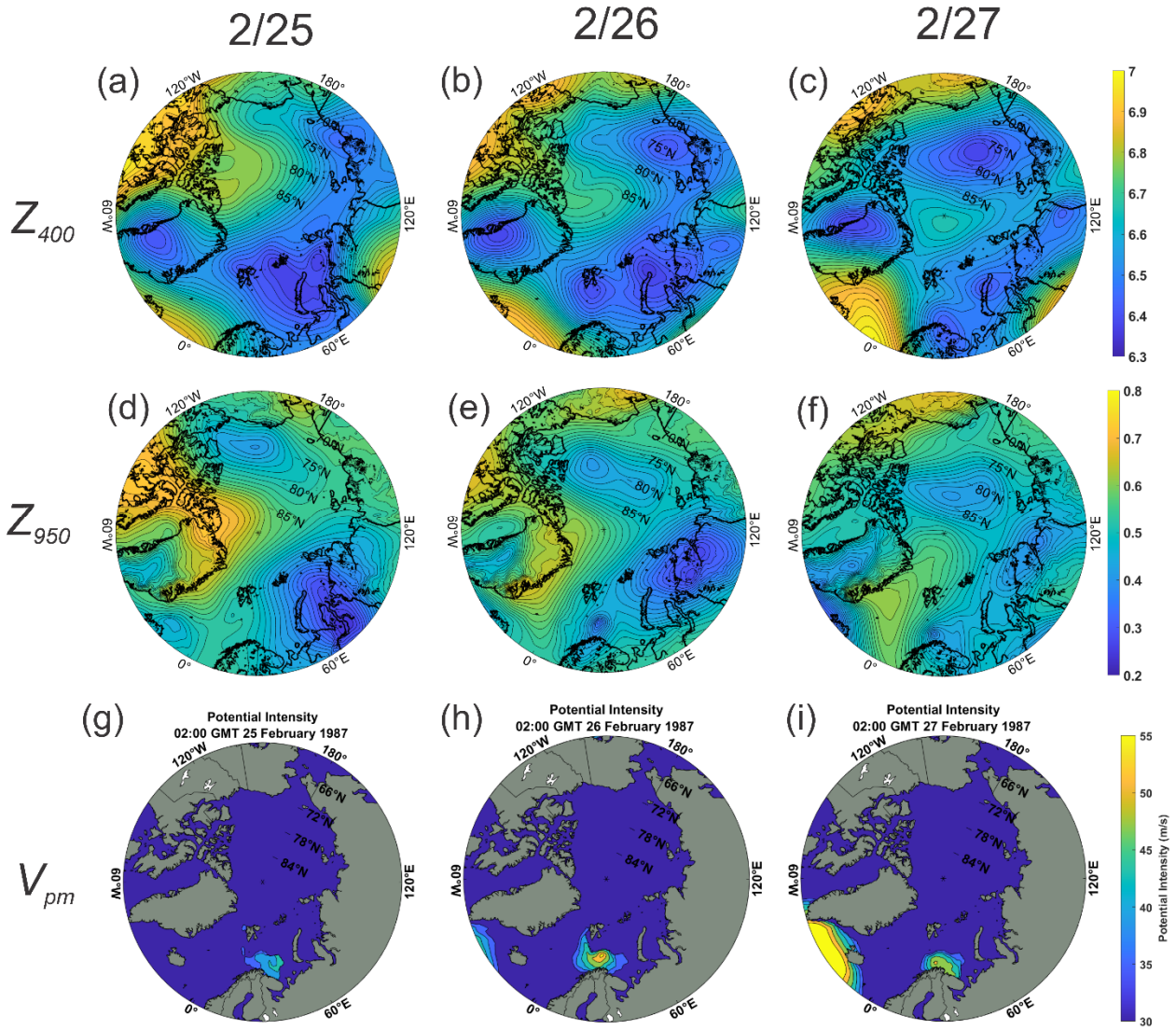
Figure 13: 400 hPa geopotential height (km)t at intervals of 23.3 m (a-c), 950 hPa geopotential height (km) in intervals of 20 m (d-f), and V_{pm} (ms^{-1}) in intervals of 4 ms^{-1} (g-i), at 02:00 UTC on February 25th (left), 26th (center), and 27th (right), 1987. From ERA-5 reanalysis.

One interesting feature of polar waters in winter is that the thermal stratification is sometimes reversed from normal, with warmer waters lying beneath cold surface waters. This is made possible, in part, by strong salinity stratification, that keeps the cold water from mixing with the warmer waters below. Therefore, it is possible for polar lows to generate warm, rather than cold, wakes, and this would feed back positively on their intensity. This seems to happen in roughly half the documented cases of polar lows in the Nordic seas (Tomita and Tanaka, 2024).

3.4 Polar low over the Sea of Japan, December, 2009

Polar lows are not uncommon in the Sea of Japan, forming when deep, cold air masses from Eurasia flow out over the relatively warm ocean. They are frequent enough to warrant a climatology (Yanase and co-authors, 2016). A satellite image of one such storm is shown in Figure 14.
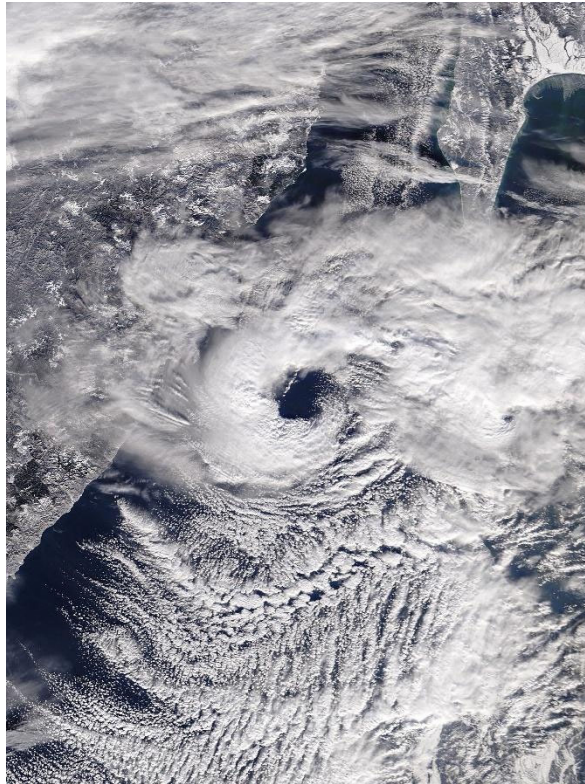
Figure 14: Polar low over the northern Sea of Japan, 02:13 UTC 20 December, 2009 as captured by the MODIS imager on NASA's Terra satellite.

The cyclone traveled almost due south from this point, striking the Hokkaido region of Japan, near Sapporo, with gale-force winds and heavy snow. As with other CYCLOPs, it formed in an environment of deep convection under a cold low aloft.

The development of the cutoff cyclone aloft was complex, as shown by the sequence of 400 hPa maps displayed in Figure 15. These are 00 UTC charts at 1-day intervals beginning on December 11th and ending on the 20th, about the time of the image in Figure 14. A large polar vortex is centered in northern central Russia on the 11th but sheds a child low southeastward on the 12th and 13th, becoming almost completely cutoff on the 14th. The parent low drifts westward during this time. The newly formed cutoff cyclone meanders around in isolation from the 15th through the 17th, but becomes wrapped up with a system propagating into the domain from the east on the 18th. By the 20th, a small-scale cutoff cyclone is drifting southward over the northern Sea of Japan, and it is this upper cutoff that spawns the polar low.

454
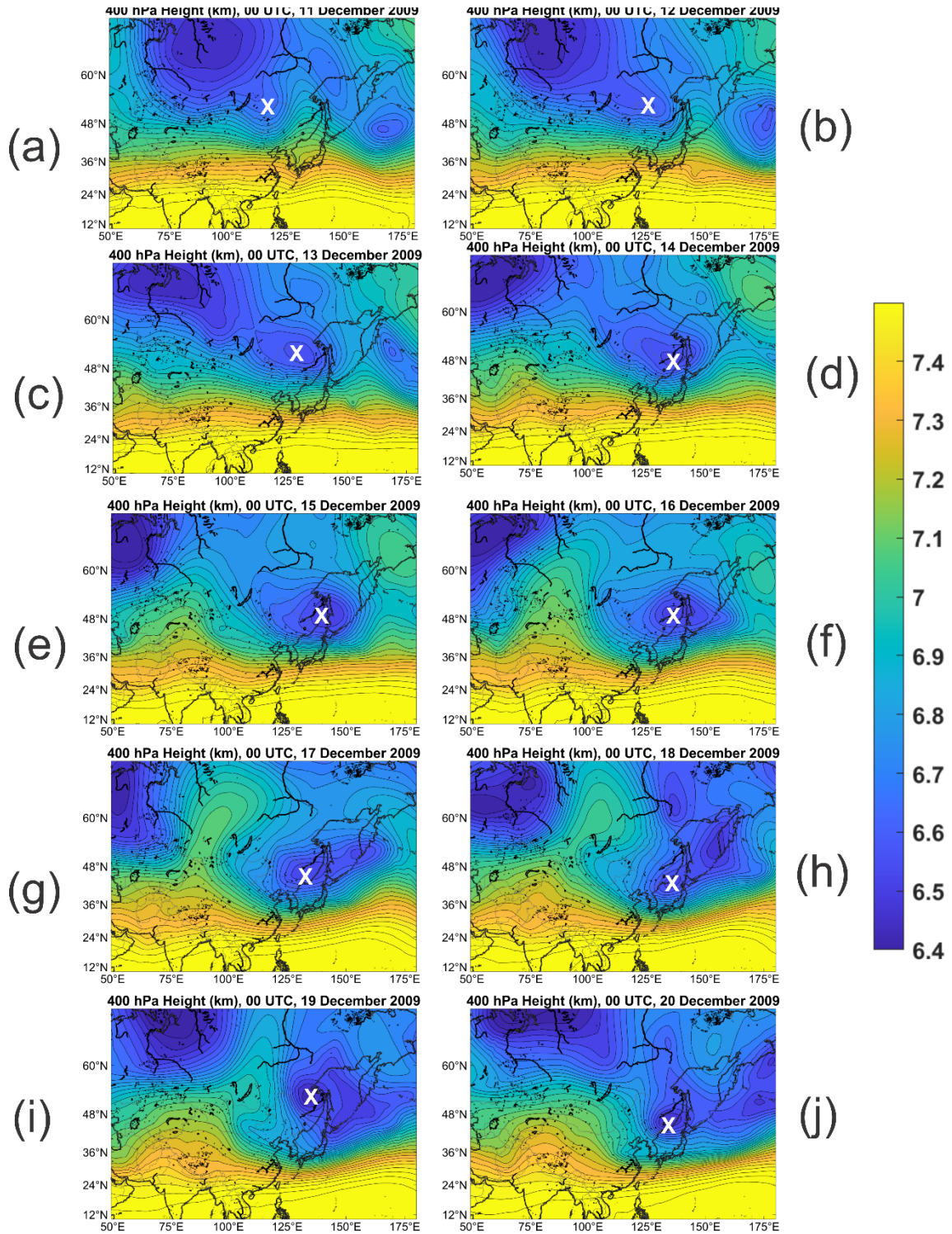
Figure 15: Sequence of 400 hPa geopotential height (km) charts at 1-day intervals from 00 UTC on December 11th
(a) to 00 UTC on December 20th (j), 2009. The charts span from 0º to 180º longitude and from 10º to 70º latitude, and
the contour increment is 36.7 m. The white crosses mark the center of the 400 hPa cyclone that was ultimately
associated with the polar low. From ERA-5 reanalysis.

459   The 950 hPa height and the V_{pm} fields at 00 UTC on December 20th are shown in Figure 16. At
460   this time, the surface low is developing rapidly and moving southward into a region of high
461   potential intensity. The latter reaches a maximum near the northwest coast of Japan, where the
462   sea surface temperatures are larger. As with the two medicane cases and the other polar low
463   case, the CYCLOP develops in a place where the potential intensity values are normally too low
464   for surface flux-driven cyclones but for which the required potential intensity is created by the
465   movement of a deep cold cyclone aloft over relatively warm water. The reanalysis 750 hPa
466   temperature (not shown) presents a local maximum at the location of the surface cyclone at this
467   time.

(a)   (b)
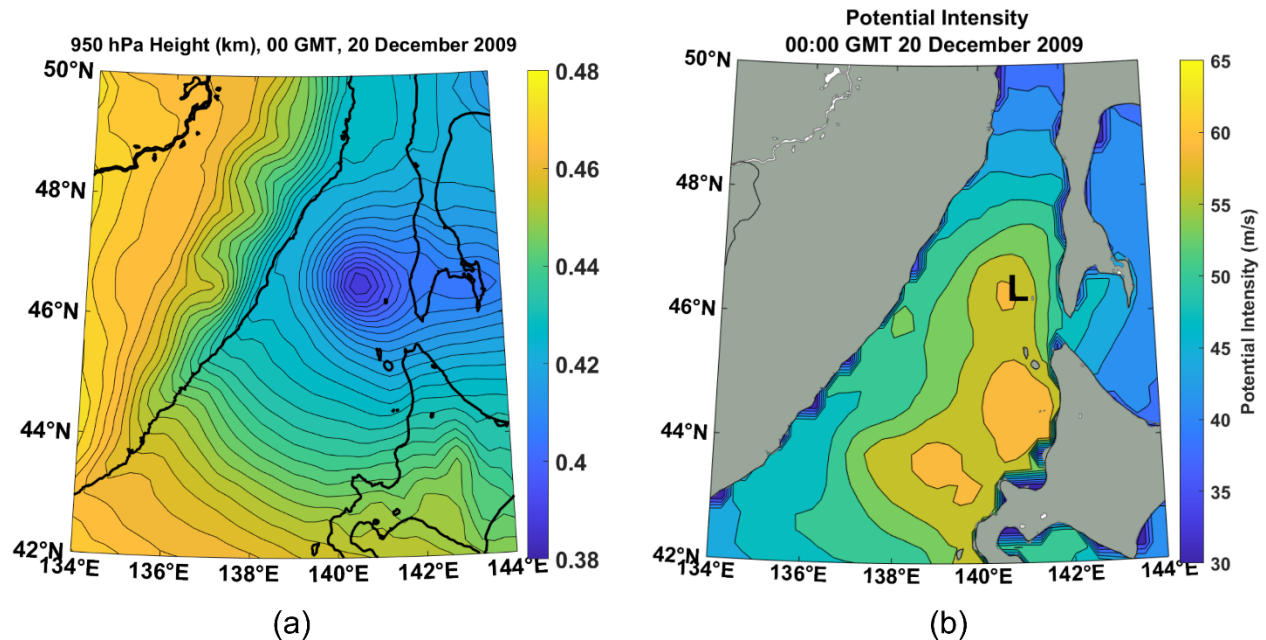
469   *Figure 16: 950 hPa geopotential height (a; km) at intervals of 3 m, and V_{pm} at intervals of 3 m s^{-1} (b), at 00 UTC on*
470   *20 December, 2009. In (b), the "L" marks the satellite-derived surface cyclone center. From ERA-5 reanalysis.*

3.5 The subtropical cyclone of January, 2023

473   The term "subtropical cyclone" has been used to describe a variety of surface flux-assisted
474   cyclonic storms that do not strictly meet the definition of a tropical cyclone. The term has an
475   official definition in the North Atlantic[5] but is used occasionally elsewhere, especially in regions
476   where terms like medicane, polar low, and Kona storm do not apply, such as the South Atlantic
477   (Evans and Braun, 2012; Gozzo et al., 2014). Here we will use the term to designate CYCLOPs
478   in the sub-arctic North Atlantic; that is, surface flux-powered cyclones that develop in regions

---

[5] The National Hurricane Center defines a "subtropical cyclone" as "a non-frontal low-pressure system
that has characteristics of both tropical and extratropical cyclones", but in the past has also used the
terms "hybrid storm" and "neutercane".

479   and times whose climatological thermodynamic potential is small or zero, that would not be
480   called polar lows owing to their latitude. This usage may not be consistent with other definitions.
481   The point here is to show that CYCLOPs can occur in the North Atlantic and we can safely refer
482   to these as CYCLOPs whether or not they meet some definition of "subtropical cyclone".

483   Figure 17 displays a visible satellite image of a subtropical cyclone over the western North
484   Atlantic on 16 January, 2023. It resembles the medicanes and polar lows described previously,
485   and like them, formed under a cutoff cyclone aloft.

486
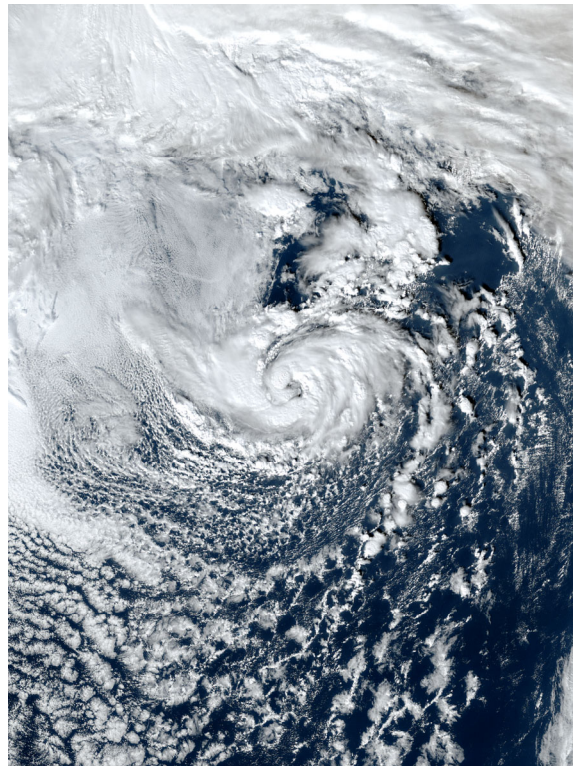
487   *Figure 17: Subtropical cyclone over the western North Atlantic, 18:20 UTC, 16 January 2023. NOAA geostationary*
488   *satellite image.*

489   The formation of the cutoff cyclone aloft is shown in Figure 18. A deep trough advances slowly
490   eastward over eastern North America and partially cuts off on the 14th. As the associated cold
491   pool and region of light shear migrate out over the warm waters south of the Gulf Stream, a
492   CYCLOP forms and intensifies with peak winds of around 60 kts at around 00 UTC on the 17th
493   (Cangliosi et al., 2023). Note also the anticyclonic wave breaking event to the east of the
494   surface cyclone development, in the eastern half of panels 18b-d.

495   The evolutions of the 950 hPa and associated V_{pm} fields are displayed in Figure 19. (Note the

496   smaller scale around the developing surface cyclone, compared to Figure 18.) On January 14th,

497   the only appreciably large values of V_{pm} are associated with the Gulf Stream and in the far

498   southwestern portion of the domain. The 950 hPa height field shows a broad trough associated

499 with the baroclinic wave moving slowly eastward off the U.S. east coast. But as the upper cold
500 cyclone moves out over warmer water on the 15th, large V_{pm} develops south of the Gulf Stream,
501 and a closed and more intense surface cyclone develops under the lowest 400 hPa heights and
502 over the region with higher V_{pm} values.

503

504
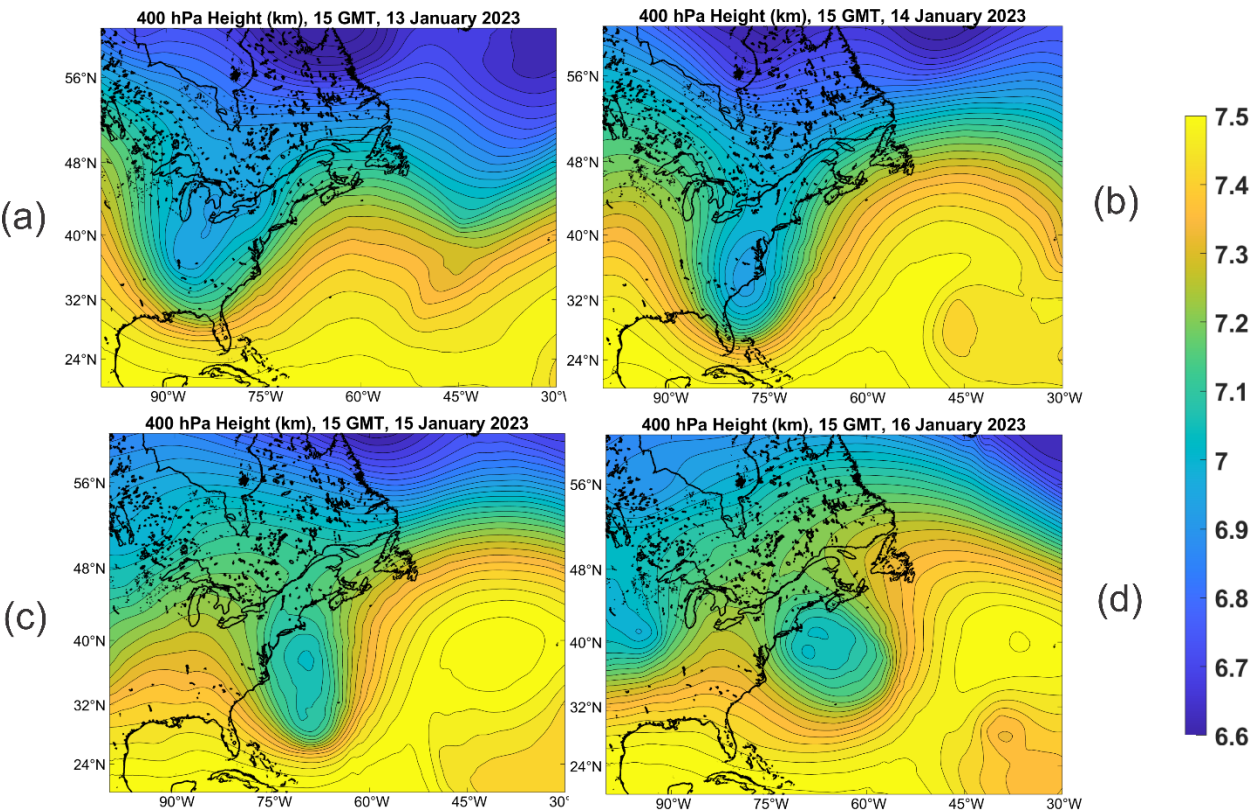
505 *Figure 18: 400 hPa geopotential height (km) at intervals of 30 m, at 15:00 UTC on January 13th (a), 14th (b), 15th (c),*
506 *and 16th (d), 2023. From ERA-5 reanalysis.*

507

(a)   (b)   (c)

(d)   (e)   (f)

508
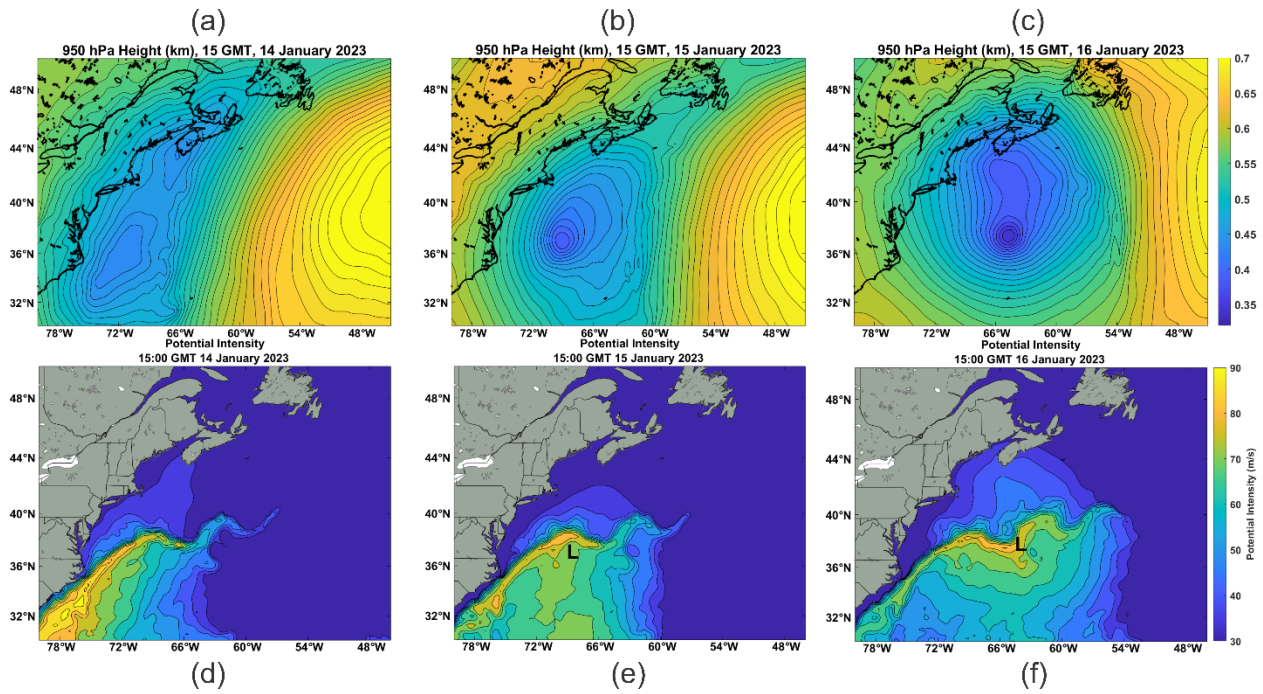
Figure 19: The 950 hPa geopotential height (km) at 15:00 UTC on January 14th (a), 15th (b), 16th (c); the V_{pm} field in increments of 5 ms^{-1}, on January 14th (d), 15th (e), and 16th(f). In (e) and (f) the "L" shows the position of the 950 hPa cyclone center at the time of the chart. From ERA-5 reanalysis.

512 As the upper tropospheric cyclone begins to pull out toward the northeast on the 16th, the
513 surface cyclone intensifies in the region of large V_{pm} south of the Gulf Stream, while the more
514 gradual warming of the surface air in the region of small V_{pm} north of the Stream yields surface
515 pressure falls, but not as concentrated and intense as in the CYCLOP to the south.

516 Although the evolution of the upper tropospheric cyclone differs in detail from the previously
517 examined cases, and the sharp gradient of sea surface temperature across the north wall of the
518 Gulfstream clearly plays a role here, in other respects the development of this subtropical
519 cyclone resembles that of other CYCLOPs, developing in regions of substantial thermodynamic
520 potential that result, at least in part, from cooling aloft on synoptic time and space scales.

521   3.6 A Kona Storm

522 Hawaiians use the term "Kona Storm" to describe cold-season storms that typically form west of
523 Hawaii and often bring damaging winds and heavy rain to the islands. The term "Kona"
524 translates to "leeward", which in this region means the west side of the islands. They may have
525 been first described in the scientific literature by Daingerfield (1921). Simpson (1952) states that
526 Kona Storms possess "cold-core characteristics, with winds and rainfall amounts increasing with
527 distance from the low-pressure center and reaching a maxima at a radius of 200 to 500 mi.
528 However, with intensification, this cyclone may develop warm-core properties, with rainfall and

529 wind profiles bearing a marked resemblance to those of the tropical cyclone." In general,
530 Simpson's descriptions of the later stages of some Kona Storms are consistent with them being
531 CYCLOPs. But it should be noted that the term is routinely applied to cold-season storms that
532 bring hazardous conditions to Hawaii regardless of whether they have developed warm cores. A
533 good review of the climatology of Kona storms is provided by Otkin and Martin (2004), who state
534 that "development of the surface cyclone in all types results from the intrusion of an upper-level
535 disturbance of extratropical origin into the subtropics". Here we focus on Kona storms that do
536 develop warm cores, providing as a first example the Kona Storm of 19 December 2010. A
537 visible satellite image of this storm is shown in Figure 20.

538
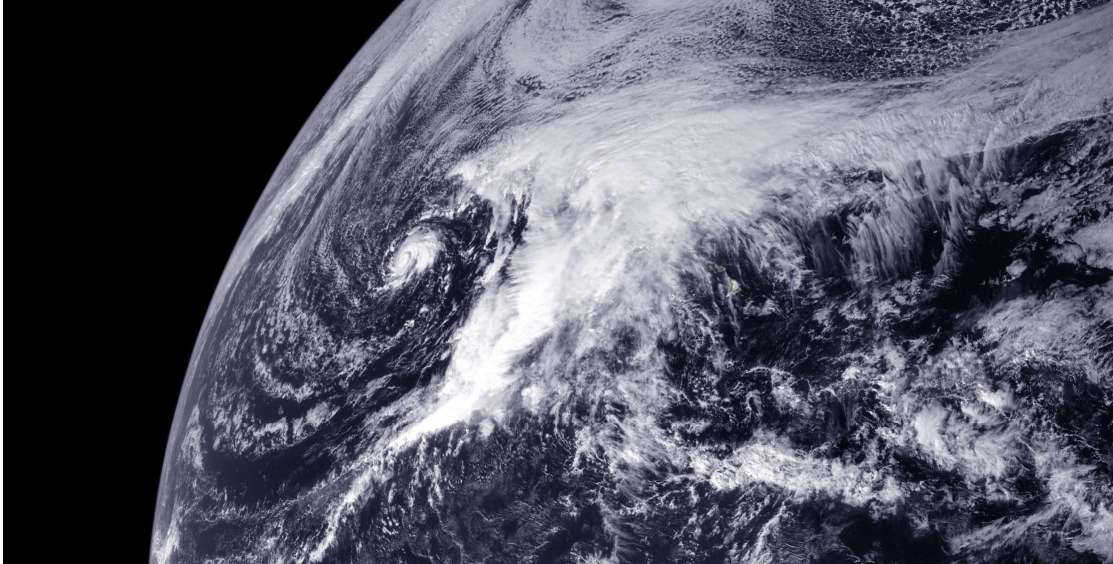
539 *Figure 20: Geostationary satellite visible image showing a Kona Storm at 00 UTC on 19 December 2010. The Kona*
540 *Storm is the small-scale cyclone left of the major cloud mass. (Image credit: NOAA-NASA GOES Project, 2010.)*

541
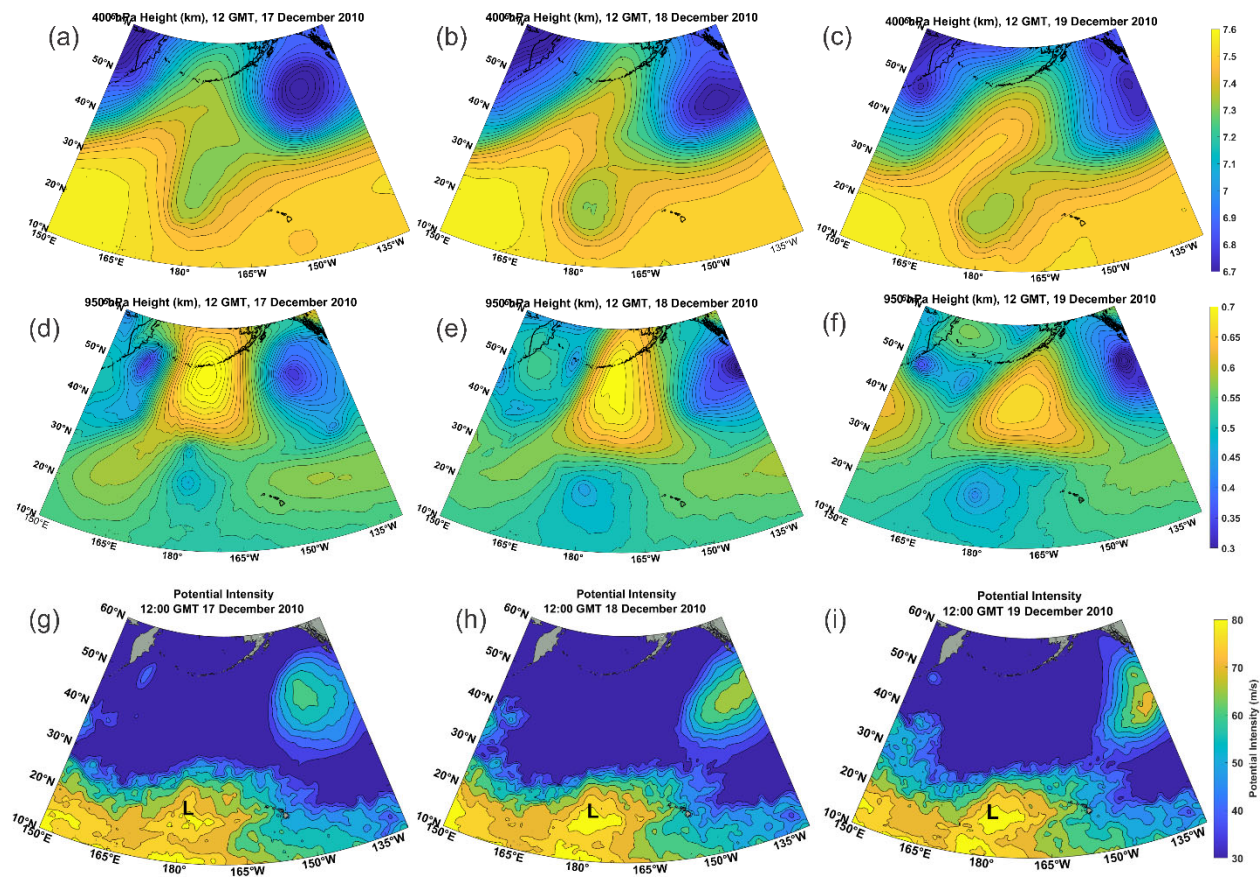
Figure 21: Sequence of 400 hPa geopotential height charts (km) at contour intervals of 30 m (a)-(c)), 950 hPa geopotential heights (km) with contour intervals of 13.34 m (d)-(f), and V_{pm} with contour intervals of 5 ms^{-1} ((g)-(i)) at 12:00 UTC on December 17th ((a), (d), (g)), December 18th ((b), (e), (h), and December 19th ((c), (f), (i)) 2010. The "L"s in ((g)-(i)) denote the positions of the 950 hPa cyclone center. From ERA-5 reanalysis.

As with all known CYCLOPs, the December 2010 Kona Storm developed under a cold-core cutoff cyclone aloft, as shown in Figure 21. The upper-level cyclone had a long and illustrious history before December 18th, having meandered over a large swath of the central North Pacific. But beginning on December 17th, the cutoff cyclone made a decisive swing southward over waters with higher values of V_{pm}. A broad surface cyclone was present underneath the cold pool aloft on all three days, but developed a tight inner core on the 19th as the cold pool slowly drifted over a region of higher potential intensity.

This Kona Storm developed in a region of modest climatological potential intensity that was, however, substantially enhanced by the cutoff cyclone aloft. For example, on December 17th, the conventional (unmodified) potential intensity at the position of the 950 hPa cyclone center was about 55 ms^{-1}, compared to the 75-80 ms^{-1} values of the modified potential intensity. One can only speculate whether a surface flux-driven cyclone would have developed without the enhanced cooling associated with the cutoff cyclone aloft.

559   This Kona storm was identified as a tropical storm by the Central Pacific Hurricane Center, as of
560   0900 UTC 20 December, and given the name Omeka.

561   The Kona Storm of March, 1951 is a more unambiguous case of a CYCLOP. Figure 22 shows
562   the 950 hPa geopotential height field on March 26, 1951. The storm, at that time, was classified
563   by the Joint Typhoon Warning Center as a tropical cyclone, but the climatological potential
564   intensity there at that time of year could not have supported any tropical cyclone. Figure 22c
565   shows that substantial V_{pm} was associated with a cutoff cyclone in the upper troposphere,
566   making possible the existence of this CYCLOP.

567
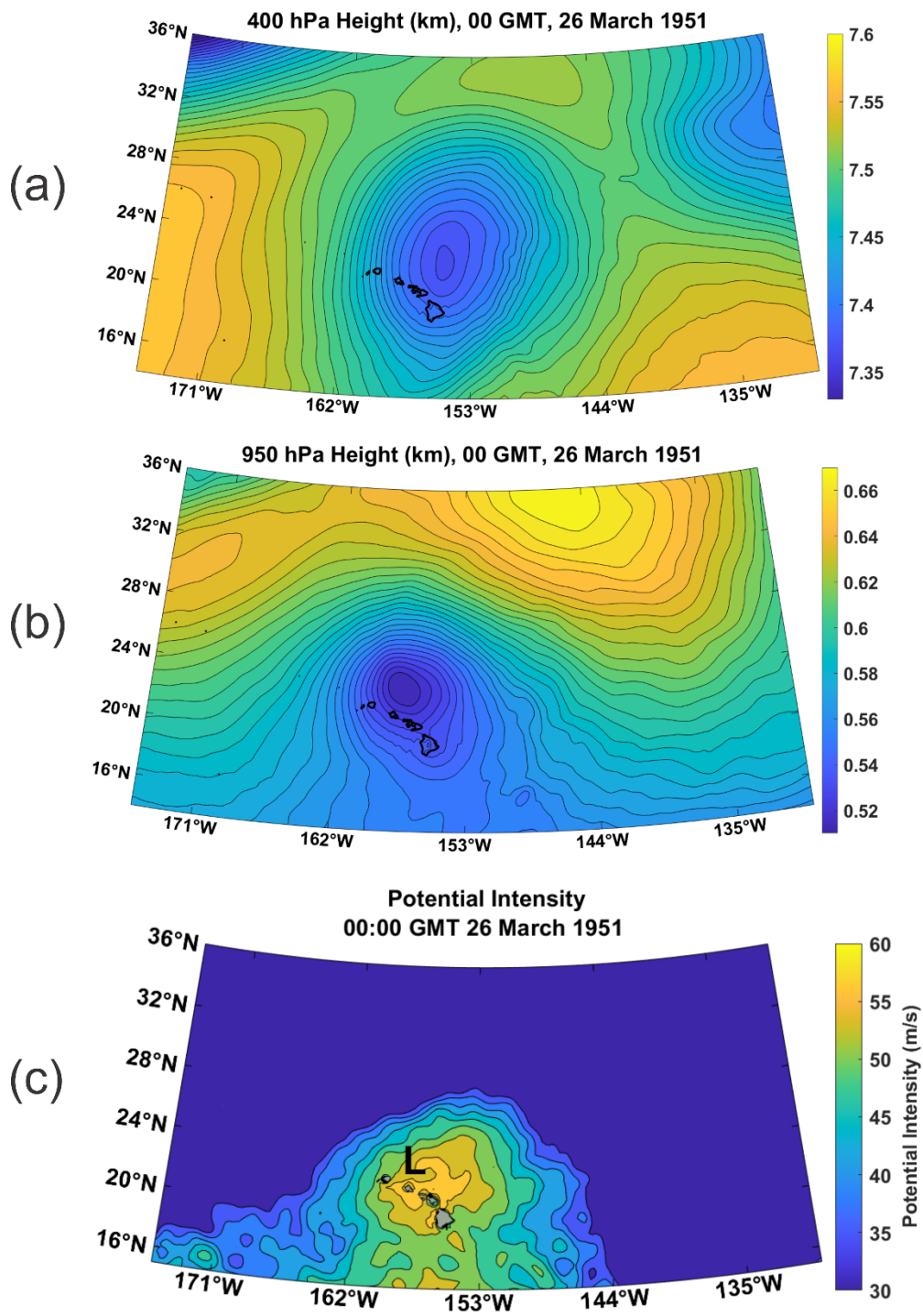
568   *Figure 22: Kona Cyclone of March, 1951. Fields are shown at 00 UTC on 26 March: a): 400 hPa geopotential height*

569   *(km)with a 10 m contour interval, b): 950 hPa geopotential height (km) with 5m contour interval, and c): V_{pm} with a*

570   *contour interval of 3 ms^{-1}.*

4. Variations on the Theme

We here are attempting to distinguish a class of cyclones, CYCLOPs, from other cyclonic storms by the physics of their development, not by the regions in which they develop. Here we present a case of an actual tropical cyclone in the Mediterranean that we do not identify as a CYCLOP.

4.1 Cyclone Zorbas

The cyclone known as Zorbas developed just north of Libya on 27 September 2018 and moved northward and then northeastward across the Peloponnese and the Aegean (Figure 23), dissipating in early October. The storm killed several people and did millions of dollars of damage.

Figure 23: Track of Cyclone Zorbas, from 27 September through 2 October, 2018. (Image credit: Wikipedia Commons; https://commons.wikimedia.org/wiki/File:Zorbas_2018_track.png)

The antecedent (actual, not modified) potential intensity distribution, on 26 September, is displayed in Figure 24. In much of the southern part of the central Mediterranean, the potential intensity was typical of tropical warm pools with values approaching 80 ms^{-1}. As with most medicanes, Zorbas was triggered by an upper tropospheric Rossby wave breaking event (Figure 25), but in this case the cold pool aloft only enhanced the existing potential intensity by about 7 ms^{-1} (on September 27th). In this case, the maximum 400 hPa geopotential perturbation was around 1500 m^{2}s^{-2}, compared to about 2500 m^{2}s^{-2} in the case of Medicane Zeo of 2005. Zorbas was therefore more like a classic case of a tropical cyclone resulting from tropical transition (Bosart and Bartlo, 1991; Davis and Bosart, 2003, 2004) and we might not describe it as a CYCLOP. Note that while the approach of the upper-level cyclone did not appreciably alter the potential intensity, it almost certainly humidified the middle troposphere, making genesis somewhat more likely, as may be true in most cases of tropical transition.

597
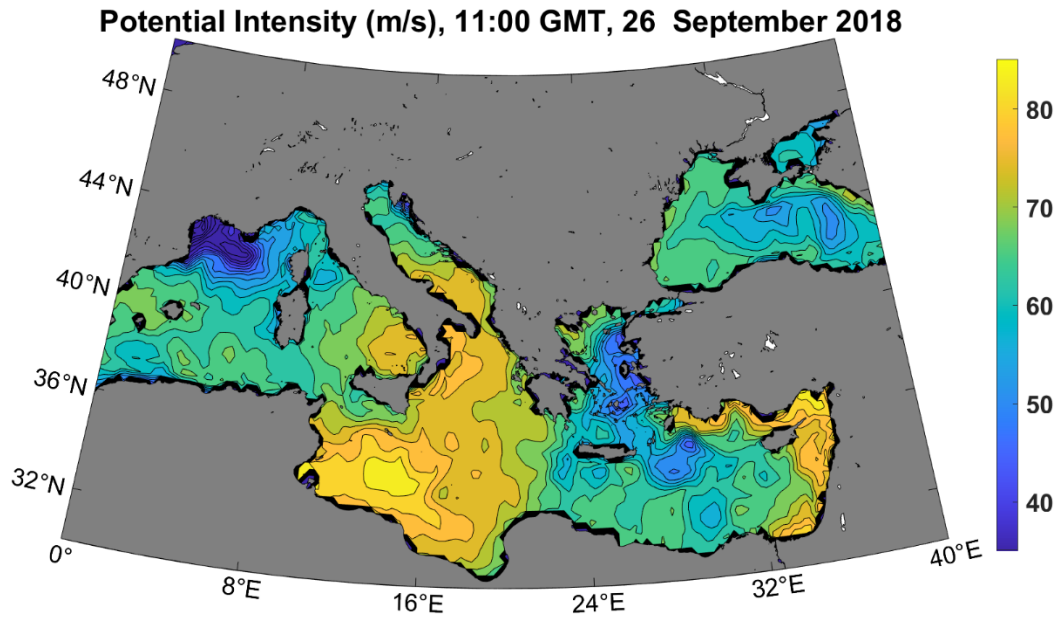
598 *Figure 24: Actual potential intensity distribution in the Mediterranean and Black Seas, 11 UTC on 26 September*
599 *2018.*

600

601
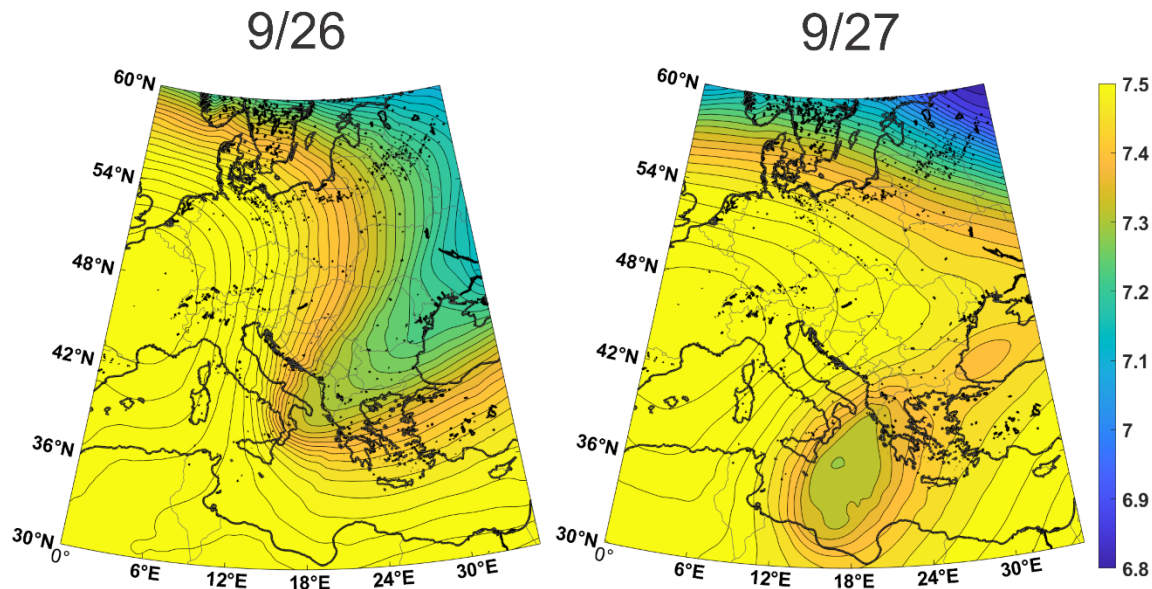
602 *Figure 25: 400 hPa geopotential height (km) at 11 UTC on 26 September (left) and 27 September (right), 2018.*
603 *Contour interval is 13.34 m. From ERA-5 reanalysis.*

604 ## 4.2 Cyclone Daniel

605 Cyclone Daniel of 2023 was the deadliest Mediterranean surface flux-driven cyclone in recorded
606 history, with a death toll exceeding 4,000 and thousands of missing persons, mostly owing to
607 floods caused by the catastrophic failure of two dams near Derna, Libya (Flaounas et al., 2024).

608   This flooding was the worst in the recorded history of the African continent. Figure 26 shows the
609   track of Daniel's center and a visible satellite image of the storm as it approached landfall in
610   Libya is shown in Figure 27. Daniel became a surface flux-driven cyclone off the west coast of
611   the Peloponnese on September 5th, made landfall near Benghazi, Libya, on September 10th and
612   dissipated over Egypt on the 12th.

613

614   *Figure 26: Track of Storm Daniel at 6-hour intervals, beginning September 5th and ending September 12th, 2023. The*
615   *circles, squares and triangles along the track denote tropical cyclone, subtropical cyclone and extratropical cyclone*
616   *designations, respectively, while the deep blue and light blue colors denote tropical depression- and tropical storm-*
617   *force winds. (Image credit: Wikipedia commons; https://commons.wikimedia.org/wiki/File:Daniel_2023_track.png)*

618
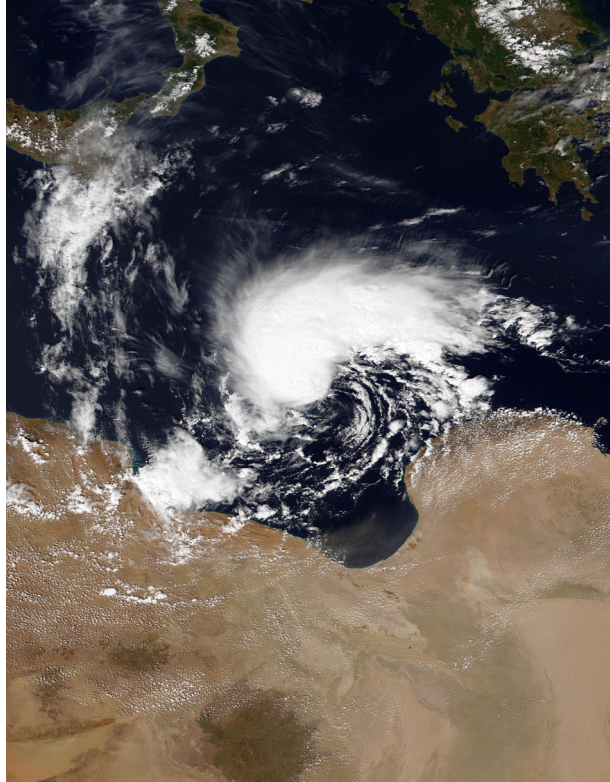
619 *Figure 27: NOAA-20 VIIRS image of Storm Daniel at 12 UTC 9 September 2023, as it approached the Libyan coast.*

620

621 As with Zorbas, the antecedent potential intensity was high throughout the Mediterranean south
622 and east of Italy and Sicily, and the event was triggered by a Rossby wave breaking event
623 (Figure 28). And as with Zorbas, the cutoff cyclone aloft was not strong enough to appreciably
624 alter the existing potential intensity but acted as a trigger for the tropical cyclone that Daniel
625 became. This was another classic case of tropical transition, and not a CYCLOP.
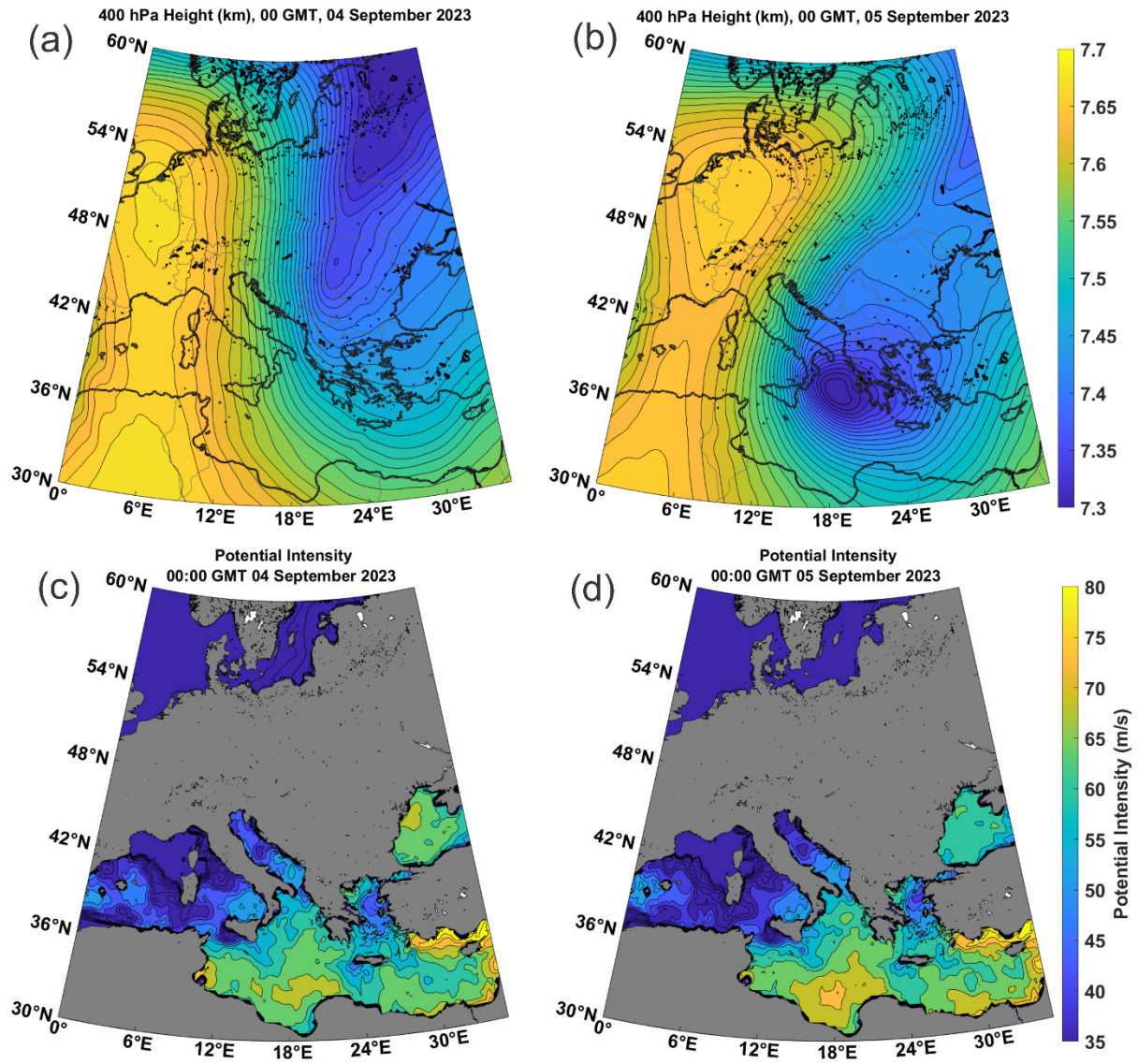
Figure 28: 400 hPa geopotential height (km) with contour interval of 13.33 m (a)-(b); and actual potential intensity (ms^{-1}) with contour interval of 4 ms^{-1} (c)-(d) at 00 UTC September 4th ((a) and (c)) and 5th ((b) and (d)), from ERA-5 reanalyses.

Yet Storm Daniel differed from Zorbas in one important respect: as it approached the Libyan coast around September 10th, it came under the influence of strong high-level potential vorticity (PV) advection owing to a mesoscale "satellite" PV mass rotating around the upper-level cutoff cyclone (Figure 29). The quasi-balanced forcing associated with the superposition of the high-level PV anomaly with the surface-based warm core probably contributed to Daniel's intensification which, remarkably for a surface flux-driven cyclone, continued after landfall (Hewson et al., 2024).
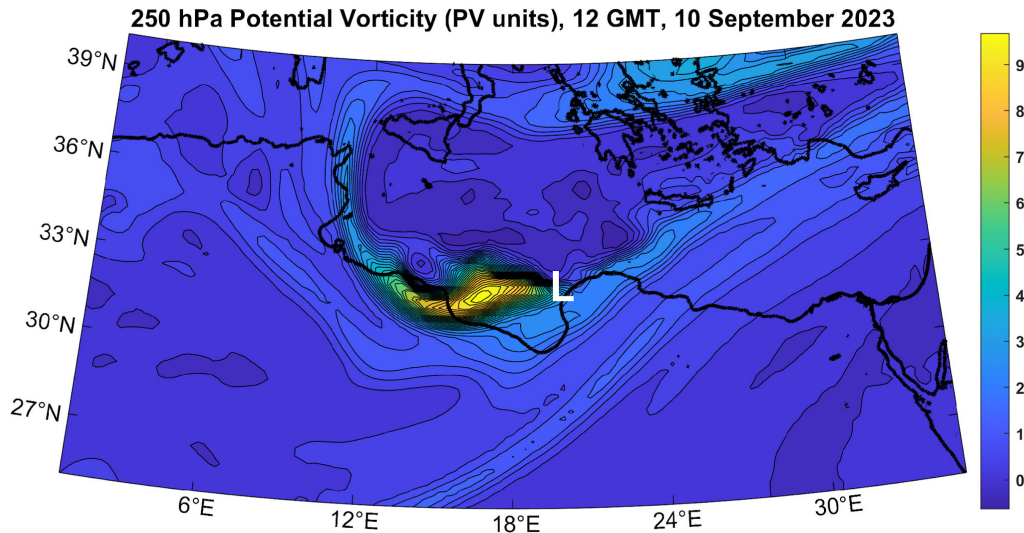
638 *Figure 29: Potential vorticity (PV units, 10^{-6} K kg^{-1} m^2 s^{-1}) at 250 hPa at 12 UTC on 10 September, 2023. The white*
639 *"L" marks the approximate surface center of Daniel at this time.*

640

5. Summary and conclusions

642 We here argue that many of the cyclonic storms called medicanes, polar lows, subtropical
643 cyclones, and Kona storms operate on the same physics and ought to be identified as a single
644 class of storms that we propose to call CYCLOPs. In their developed structure and intensity
645 they are essentially identical to tropical cyclones, and like TCs are driven primarily by wind-
646 dependent surface enthalpy (latent and sensible heat) fluxes, but unlike classical TCs, there is
647 little or no climatological potential intensity for the storms. Rather, the development and/or
648 migration over relatively warm water of strong, cold-core cyclones in the upper troposphere
649 cools and moistens the column through dynamical lifting, generating mesoscale to synoptic
650 scale columns with elevated potential intensity and humidity, and reduced wind shear – ideal
651 embryos for the development of surface flux-driven cyclones.

652 We do not expect CYCLOPs to last as long as classical TCs. In the first place, the conditions
653 that enable such storms are confined in space and transient in time. For example, the cutoff
654 cyclone aloft is often re-absorbed into the main baroclinic flow. In addition, the strong surface
655 enthalpy fluxes that power CYCLOPs also increase, through the action of deep convection, the
656 enthalpy of the otherwise spatially limited cold columns in which they form, reducing over time
657 the thermodynamic disequilibrium between the air column and the sea surface. A back-of-the-
658 envelope estimate for the time to destroy the initial thermodynamic disequilibrium is on the order
659 of days. By contrast, even the strongest classical TCs do not sufficiently warm the large
660 expanses of the tropical troposphere they influence to appreciably diminish the large-scale
661 potential intensity of tropical warm pools.

662   Not all cyclonic storms that have been called polar lows, medicanes, subtropical cyclones, or
663   Kona storms meet our definition of CYCLOP. The literature describes many polar lows that have
664   been traced to something more nearly like classical baroclinic instability acting in an air mass of
665   anomalously low static stability (e.g. Sardie and Warner, 1985). Many storms identified as Kona
666   storms because of their location and season, and which developed under cold cyclones aloft,
667   never received much of a boost from surface fluxes and therefore would not be classified as
668   CYCLOPs. And, as we described in the last section, two strong Mediterranean cyclones, Zorbas
669   of 2018 and Daniel of 2023, developed in environments of high climatological potential intensity
670   and formed via the tropical transition process.

671   Beyond these caveats, not all cold-core, closed cyclones in the upper troposphere that develop
672   or move over relatively warm ocean waters develop CYCLOPs. Without doing a comprehensive
673   survey, we have found several cases of greatly enhanced potential intensity under cold lows
674   aloft that did not develop strong, concentrated surface cyclones. We suspect that, as with
675   classical tropical cyclones, dry air incursions above the boundary layer may have prevented
676   genesis in these cases, but as these events generally occur in regions devoid of in-situ
677   observations, it is not clear how well reanalyses capture variations of moisture on the scale of
678   CYCLOPs. In any event, the efficiency with which upper-level cut-off cyclones produce
679   CYCLOPs, given a substantial perturbation in potential intensity, should be a subject of future
680   research.

681   Clearly, there exists a continuum between pure tropical transition, in which synoptic-scale
682   dynamics play no role in setting up the potential intensity, and pure CYCLOPs in which
683   synoptic-scale processes create all the potential intensity that drives the storm. The distinction
684   we are making here does not pertain to the final result – a tropical cyclone[6] – but to the route to
685   creating it. As a practical matter, forecasters should consider both the triggering potential and
686   mesoscale to synoptic scale environmental development in predicting the formation and
687   evolution of CYCLOPs. The modified potential intensity (V_{pm}) introduced here may prove to be
688   a valuable diagnostic that can easily be calculated from NWP model output. To simulate
689   CYCLOPs, NWP models need to make accurate forecasts of dynamic processes that lead to
690   the formation and humidification of deep cold pools aloft, and be able to handle surface fluxes
691   and other boundary layer processes essential to the formation of surface flux-driven cyclones.
692   And, as with tropical cyclones, coupling to the ocean is essential for accurate intensity
693   prediction.

694   Finally, we encourage researchers to focus on the essential physics of CYCLOP development
695   regardless of where in the world they occur. Casting a broader geographical net will harvest a
696   greater sample of such storms and should lead to more rapid progress in understanding and
697   forecasting them.

---

[6] It might be beneficial to develop a term that generically denotes a cyclone driven primarily by surface enthalpy fluxes. "Tropical cyclone" seems unsuited to the task, since "tropical" hardly describes, e.g., a polar low. Such a generic term would encompass both conventional tropical cyclones, which occur in regions of climatologically large potential intensity, and CYCLOPs, for which potential intensity is generated locally in space and time.

Appendix

699 CYCLOPs form when dynamical processes create synoptic-scale cold columns marked by
700 cutoff cyclones in the upper troposphere. The objective here is to calculate tropical cyclone
701 potential intensity in these cold columns. The problem is that the CYCLOPs themselves, and
702 surface heat fluxes in general, warm the columns, sometimes rapidly, diminishing the potential
703 intensity. We want to know what the potential intensity was before this warming occurs. Here we
704 develop a modified potential intensity using the surface pressure depression as proxy for the
705 column heating.

706 Potential intensity is a measure of the maximum surface wind speed that can be achieved by a
707 cyclone fueled entirely by surface enthalpy fluxes. It is defined (see Rousseau-Rizzi and
708 Emanuel (2019) for an up-to-date definition):

709
$$V_p^2 = \frac{C_k}{C_D} \frac{T_s - T_o}{T_o} \left(h_0^* - h_b \right),$$
(A1)

710 Where C_k and C_D are the surface exchange coefficients for enthalpy and momentum, T_s and

711 T_o are the absolute temperatures of the surface and outflow layer, h_0^* is the saturation moist

712 static energy of the sea surface, and h_b is the moist static energy of the boundary layer.

713 Using the relation $T\delta s \simeq \delta h$, where s is moist entropy, we can re-write (A1) slightly as

714
$$V_p^2 = \frac{C_k}{C_D} \frac{T_s - T_o}{T_o} T_s \left(s_0^* - s_b \right).$$
(A2)

715 Next, we assume that the troposphere near CYCLOPs has a nearly moist adiabatic lapse rate[7],
716 and the moist entropy of the boundary layer is equal to the saturation moist entropy, s^*, of the
717 troposphere; i.e., that the troposphere is neutrally stable to moist adiabatic ascent from the
718 boundary layer. Under these conditions, (A2) may be re-written

719
$$V_p^2 = \frac{C_k}{C_D} \frac{T_s - T_o}{T_o} T_s \left(s_0^* - s^* \right).$$
(A3)

720 Here s^* is constant with altitude, since the troposphere is assumed to have a moist adiabatic
721 lapse rate.

---

[7] If the lapse rate is appreciably sub-adiabatic, then convection cannot occur and no flux-driven cyclone could develop. This condition would be associated with a larger value of s* in (A3), which would at least reduce the calculated value of V_p. Super-adiabatic lapse rates are not generally observed over the ocean within deep humid layers.

722 Referring to Figure 1a in the main text, we want to know what the potential intensity is in the
723 vicinity of the cutoff cyclone aloft *before* the atmosphere underneath it has started to warm up
724 under the influence of surface enthalpy fluxes. But in reality, this warming commences as soon
725 as the system moves over relatively warm water and deep convection begins. We can estimate
726 what the temperature, or s^*, was before the warming began by using the surface pressure drop
727 as a proxy for the column warming.

728 We begin with the perturbation hydrostatic equation in pressure coordinates:

$$\frac{\partial \phi'}{\partial p} = -\alpha', \qquad (A4)$$

730 where ϕ' is the perturbation geopotential and α' is the perturbation specific volume. Since the
731 latter is a function of pressure and s^* only, we can use the chain rule and one of the Maxwell
732 relations from thermodynamics (Emanuel, 1994) to write (A4) as

$$\frac{\partial \phi'}{\partial p} = -\left(\frac{\partial T}{\partial p}\right)_{s^*} s^{*\,'}. \qquad (A5)$$

734 Now, since $s^{*\,'}$ does not vary with altitude, we can integrate (A5) from the surface to the local
735 tropopause to yield

$$-\phi_s' = \left(T_s - T_{\phi'=0}\right) s^{*\,'}. \qquad (A6)$$

737 where ϕ_s' is the near-surface geopotential perturbation and $T_{\phi'=0}$ is the absolute temperature at
738 the level where the CYCLOP-induced geopotential perturbation vanishes.

739 Therefore the CYCLOP-induced warming of the troposphere is estimated as

$$s^{*\,'} = \frac{-\phi_s'}{T_s - T_{\phi'=0}}. \qquad (A7)$$

741 We subtract this warming from the reanalysis environmental saturation entropy in (A3), yielding

$$V_{pm}^2 = \frac{C_k}{C_D} \frac{T_s - T_o}{T_o} T_s \left(s_0^* - s_e^* - \frac{\phi_s'}{T_s - T_{\phi'=0}}\right), \qquad (A8)$$

743 where s_e^* is the analyzed saturation entropy of the column. This can be written alternatively as

$$V_{pm}^2 = V_p^2 - \frac{C_k}{C_D} \frac{T_s}{T_o} \frac{T_s - T_o}{T_s - T_{\phi'=0}} \phi_s', \qquad (A9)$$

745   where V_p is the potential intensity calculated from the reanalysis. We use (A9) in the

746   calculations reported in this paper, with V_p calculated using the algorithm of Bister and Emanuel

747   (2002).

748   For the purposes of the present work, we defined the perturbation as the difference between the
749   actual geopotential and its climatological value determined from monthly mean values over the
750   period 1979-2023, and we estimate the near-surface cyclone geopotential perturbation as that
751   at 950 hPa. In (A9), we do not know the precise value of $C_k / C_D,$ but it should be of order unity
752   and is generally assumed as such when potential intensity is calculated in practice (e.g.
753   Emanuel, 2000). The surface temperature, $T_s,$ should be captured well in reanalyses, while the
754   outflow temperature is often taken as the local unperturbed tropopause temperature (Emanuel,
755   2000). In general, the pressure perturbation associated with tropical cyclones changes sign
756   somewhere in the upper troposphere, and for simplicity we take $T_{\phi'=0} = T_o$ here.   In the tropics,
757   the surface temperature can be around 300 K while the tropopause is often as cold as 200K,
758   yielding $T_s / T_o = 1.5,$ while in polar latitudes, the surface temperature can be just above freezing
759   (273 K) while the tropopause is warmer, around 220 K, giving $T_s / T_o = 1.25.$ As in any case
760   C_k / C_D is uncertain, we take $T_s / T_o = 1.3$ here for simplicity, and approximate (A9) as

761
$$V_{pm}^2 = V_p^2 - 1.3\,\phi_s'. \tag{A10}$$

762   The contribution of the last term in (A10) is usually small except in the immediate vicinity of a
763   CYCLOP.

764   The individual contributions of the two terms on the right side of (A10) are displayed in Figure
765   A1, which pertains to the case of Medicane Celeno on the 14th and 15th of January, 1995. The
766   total (modified) potential intensity for these two dates and times is shown in Figure 5 *g* and *h*. In
767   general, the contribution of the correction (last term in (A10)) is modest.

768   Code and data availability

769   No modeling was performed in the course of this work, and no code developed except to plot
770   reanalysis data. Routines for calculating potential intensity are available at
771   https://github.com/dgilford/tcpyPI . All of the meteorological analyses presented herein are
772   based in ERA5 downloaded from the Copernicus Climate Change Service
773   (https://doi.org/10.24381/cds.143582cf, Hersbach et al., 2020).

774   Author contributions

775   KE carried out the analyses and prepared the manuscript with contributions from all the co-
776   authors.
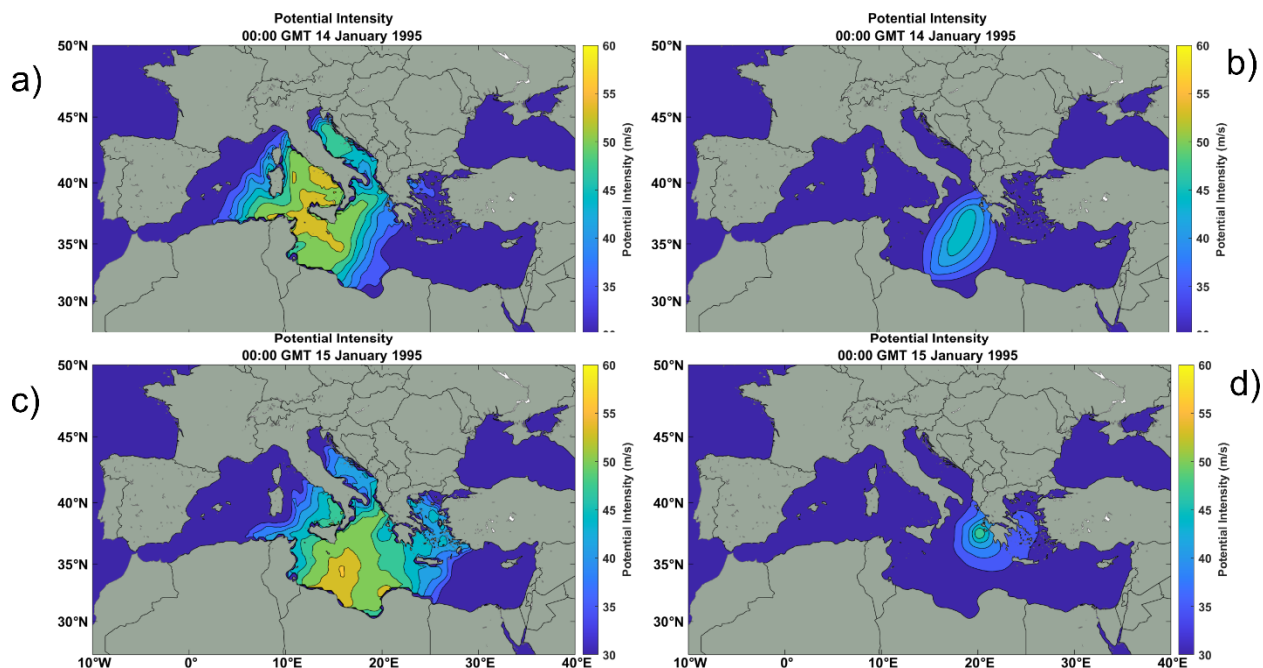
778 *Figure A1: Unmodified potential intensity (a and c) and modification of the potential intensity (b and d) at 00 UTC on*
779 *January 14th (a and b) and 15th (c and d). Note that the full modified potential intensity is not the arithmetic sum of*
780 *these two contributions but rather their Euclidean norm.*

Competing interests

The authors declare that they have no conflict of interest.

Acknowledgements

We thank two anonymous reviewers for most helpful and conscientious reviews, and Lance Bosart for his detailed and highly constructive comments.

This paper was motivated by discussions at the TROPICANA (TROPIcal Cyclones in ANthropocene: physics, simulations & Attribution) program, which took place in June 2024 at the Institute Pascal, University of Paris-Saclay, and aimed to address complex issues related to tropical cyclones, medicanes, and their connection with climate change.

This work was made possible by Institut Pascal at Université Paris-Saclay with the support of the program TROPICANA, "Investissements d'avenir" ANR-11-IDEX-0003-01.

T. Alberti and D. Faranda acknowledge useful discussions within the MedCyclones COST Action (CA19109) and the FutureMed COST Action (CA22162) communities.

S. Bourdin received financial support from the NERC-NSF research grant n° NE/W009587/1 (NERC) & AGS-2244917 (NSF) HUrricane Risk Amplification and Changing North Atlantic Natural disasters (Huracan), and from the EUR IPSL-Climate Graduate School through the

797   ICOCYCLONES2 project, managed by the ANR under the "Investissements d'avenir"
798   programme with the reference 37 ANR-11-IDEX-0004 - 17-EURE-0006.

799   S.J. Camargo and C.-Y. Lee acknowledge the support of the U.S. National Science Foundation
800   (AGS 20-43142, 22-17618, 22-44918) and U.S. Department of Energy (DOE) (DE-
801   SC0023333).

802   D. Faranda, E. Flaounas were supported by the COST Action CA22162 - FutureMed: A
803   TRANSDISCIPLINARY NETWORK TO BRIDGE CLIMATE SCIENCE AND IMPACTS ON
804   SOCIETY (FutureMed).

805   K. Emanuel was supported by the U.S. National Science Foundation under grant AGS-2202785.

806   J.J. González-Alemán thanks support from AEMET and from the Spanish PID2023-146344OB-
807   I00 project, funded by MICIU/AEI/10.13039/501100011033 y by FEDER, EU

808   M. M. Miglietta was partly supported by "Earth Observations as a cornerstone to the
809   understanding and prediction of tropical like cyclone risk in the Mediterranean (MEDICANES)",
810   ESA Contract No. 4000144111/23/I-KE.

811   H. Ramsay acknowledges funding support from the Australian Climate Service and the Climate
812   Systems Hub of the Australian Government's National Environmental Science Program (NESP).

813   M. Reale was supported by the National Recovery and Resilience Plan project TeRABIT
814   (Terabit network for Research and Academic Big data in Italy - IR0000022 - PNRR Missione 4,
815   Componente 2, Investimento 3.1 CUP I53C21000370006) in the frame of the European Union -
816   NextGenerationEU funding.

817   R. Romero acknowledges financial support by the "Ministerio de Ciencia e Innovación" of Spain
818   through the grant TRAMPAS (PID2020-113036RB-I00/AEI/10.13039/501100011033).

819

820   # References

821   Betts, A. K.: A new convective adjustment scheme. Part I: Observational and theoretical basis.,
822   Quart J Roy Meteor Soc, 112, 677-691., 1986.

823   Bister, M. and Emanuel, K. A.: Low frequency variability of tropical cyclone potential intensity, 1:
824   Interannual to interdecadel variability, J Geophys Res, 107, doi:10.1029/2001JD000776, 2002.

825   Boettcher, M. and Wernli, H.: A 10-yr climatology of diabatic Rossby waves in the northern
826   hemisphere, Mon. Weather Rev., 141, 1139–1154, https://doi.org/10.1175/MWR-D-12-00012.1,
827   2013.

828   Bosart, L. F. and Bartlo, J. A.: Tropical storm formation in a baroclinic environment, Mon Wea
829   Rev, 119, 1979–2013, 1991.

830   Cangliosi, J. P., Papin, P., and Beven, J. L.: Unnamed tropical storm (AL012023)., 2023.

831   Cavicchia, L., von Storch, H., and Gualdi, S.: A long-term climatology of medicanes, Clim. Dyn.,
832   43, 1183–1195, https://doi.org/10.1007/s00382-013-1893-7, 2014.

833   Cavicchia, L., Pepler, A., Dowdy, A., and Walsh, K.: A physically based climatology of the
834   occurrence and intensification of Australian East Coast Lows, J. Clim., 32, 2823–2841,
835   https://doi.org/10.1175/JCLI-D-18-0549.1, 2019.

836   Chavas, D. R. and Emanuel, K. A.: Equilibrium tropical cyclone size in an idealized state of
837   axisymmetric radiative–convective equilibrium, J Atmos Sci, 71, 1663–1680, 2014.

838   Cronin, T. W. and Chavas, D. R.: Dry and semidry tropical cyclones, J. Atmospheric Sci., 76,
839   2193–2212, https://doi.org/10.1175/jas-d-18-0357.1, 2019.

840   Daingerfield, L. H.: Kona storms, Mon. Weather Rev., 49, 327–329,
841   https://doi.org/10.1175/1520-0493(1921)49<327:ks>2.0.co;2, 1921.

842   Davis, C. A. and Bosart, L. F.: Baroclinically induced tropical cyclogenesis, Mon. Weather Rev.,
843   131, 2730–2747, https://doi.org/10.1175/1520-0493(2003)131<2730:BITC>2.0.CO;2, 2003.

844   Davis, C. A. and Bosart, L. F.: The TT problem: Forecasting the tropical transition of cyclones,
845   Bull. Am. Meteorol. Soc., 85, 1657–1662, https://doi.org/10.1175/BAMS-85-11-1657, 2004.

846   Emanuel, K.: Genesis and maintenance of "Mediterranean hurricanes," Adv Geosci, 2, 217–
847   220, 2005.

848   Emanuel, K.: Tropical cyclone activity downscaled from NOAA-CIRES reanalysis, 1908-1958, J
849   Adv Model Earth Sys, 2, 1–12, 2010.

850   Emanuel, K. A.: Atmospheric Convection, Oxford Univ. Press, New York, 580 pp., 1994.

851   Emanuel, K. A.: Some aspects of hurricane inner-core dynamics and energetics., J Atmos Sci,
852   54, 1014–1026, 1997.

853   Emanuel, K. A.: A statistical analysis of tropical cyclone intensity, Mon Wea Rev, 128, 1139–
854   1152, 2000.

855   Emanuel, K. A., Neelin, J. D., and Bretherton, C. S.: On large-scale circulations in convecting
856   atmospheres, Quart J Roy Meteor Soc, 120, 1111–1143, 1994.

857   Evans, J. L. and Braun, A.: A climatology of subtropical cyclones in the South Atlantic, J. Clim.,
858   25, 7328–7340, https://doi.org/10.1175/JCLI-D-11-00212.1, 2012.

859   Fantini, M.: The influence of heat and moisture fluxes from the ocean on the development of
860   baroclinic waves, J. Atmospheric Sci., 47, 840–855, https://doi.org/10.1175/1520-
861   0469(1990)047<0840:TIOHAM>2.0.CO;2, 1990.

Fita, L. and Flaounas, E.: Medicanes as subtropical cyclones: the December 2005 case from the perspective of surface pressure tendency diagnostics and atmospheric water budget, Q. J. R. Meteorol. Soc., 144, 1028–1044, https://doi.org/10.1002/qj.3273, 2018.

Flaounas, E., Dafis, S., Davolio, S., Faranda, D., Ferrarin, C., Hartmuth, K., Hochman, A., Koutroulis, A., Khodayar, S., Miglietta, M. M., Pantillon, F., Patlakas, P., Sprenger, M., and Thurnherr, I.: Dynamics, predictability, impacts, and climate change considerations of the catastrophic Mediterranean Storm Daniel (2023), EGUsphere, 2024, 1–29, https://doi.org/10.5194/egusphere-2024-2809, 2024.

Gan, M. A. and Piva, E. D.: Energetics of southeastern Pacific cut-off lows, Clim. Dyn., 46, 3453–3462, https://doi.org/10.1007/s00382-015-2779-7, 2016.

Gozzo, L. F., Rocha, R. P. da, Reboita, M. S., and Sugahara, S.: Subtropical cyclones over the southwestern South Atlantic: Climatological aspects and case study, J. Clim., 27, 8543–8562, https://doi.org/10.1175/JCLI-D-14-00149.1, 2014.

Hersbach, H., Bell, B., Berrisford, P., Hirahara, S., Horányi, A., Muñoz-Sabater, J., Nicolas, J., Peubey, C., Radu, R., Schepers, D., Simmons, A., Soci, C., Abdalla, S., Abellan, X., Balsamo, G., Bechtold, P., Biavati, G., Bidlot, J., Bonavita, M., De Chiara, G., Dahlgren, P., Dee, D., Diamantakis, M., Dragani, R., Flemming, J., Forbes, R., Fuentes, M., Geer, A., Haimberger, L., Healy, S., Hogan, R. J., Hólm, E., Janisková, M., Keeley, S., Laloyaux, P., Lopez, P., Lupu, C., Radnoti, G., de Rosnay, P., Rozum, I., Vamborg, F., Villaume, S., and Thépaut, J.-N.: The ERA5 global reanalysis, Q. J. R. Meteorol. Soc., 146, 1999–2049, https://doi.org/10.1002/qj.3803, 2020.

Hewson, T., Ashoor, A., Bousetta, S., Emanuel, K., Lagouvardos, K., Lavers, D., Magnusson, L., Pillosu, F., and Zoster, E.: Medicane Daniel: an extraordinary cyclone with devastating impacts, ECMWF Newsl., 179, 33–47, 2024.

Holland, G. J., Lynch, A. H., and Leslie, L. M.: Australian east-coast cyclones. Part I: Synoptic overview and case study, Mon. Weather Rev., 115, 3024–3036, https://doi.org/10.1175/1520-0493(1987)115<3024:AECCPI>2.0.CO;2, 1987.

Kohl, M. and O'Gorman, P. A.: The diabatic rossby vortex: growth rate, length scale, and the wave–vortex transition, J. Atmospheric Sci., 79, 2739–2755, https://doi.org/10.1175/JAS-D-22-0022.1, 2022.

Leutbecher, M. and Palmer, T. N.: Ensemble forecasting, Predict. Weather Clim. Extreme Events, 227, 3515–3539, https://doi.org/10.1016/j.jcp.2007.02.014, 2008.

McIntyre, M. E. and Palmer, T. N.: Breaking planetary waves in the stratosphere, Nature, 305, 593–600, https://doi.org/10.1038/305593a0, 1983.

McTaggart-Cowan, R., Deane, G. D., Bosart, L. F., Davis, C. A., and Galarneau, T. J.: Climatology of tropical cyclogenesis in the North Atlantic (1948–2004), Mon. Weather Rev., 136, 1284–1304, https://doi.org/10.1175/2007MWR2245.1, 2008.

899   McTaggart-Cowan, R., Galarneau, T. J., Bosart, L. F., Moore, R. W., and Martius, O.: A global
900   climatology of baroclinically influenced tropical cyclogenesis, Mon. Weather Rev., 141, 1963–
901   1989, https://doi.org/10.1175/MWR-D-12-00186.1, 2013.

902   McTaggart-Cowan, R., Davies, E. L., Fairman, J. G., Galarneau, T. J., and Schultz, D. M.:
903   Revisiting the 26.5°c sea surface temperature threshold for tropical cyclone development, Bull.
904   Am. Meteorol. Soc., 96, 1929–1943, https://doi.org/10.1175/BAMS-D-13-00254.1, 2015.

905   Miglietta, M. M. and Rotunno, R.: Development mechanisms for Mediterranean tropical-like
906   cyclones (medicanes), Q. J. R. Meteorol. Soc., 145, 1444–1460, https://doi.org/10.1002/qj.3503,
907   2019.

908   Nastos, P. T., Karavana Papadimou, K., and Matsangouras, I. T.: Mediterranean tropical-like
909   cyclones: Impacts and composite daily means and anomalies of synoptic patterns, High Impact
910   Atmospheric Process. Mediterr., 208, 156–166, https://doi.org/10.1016/j.atmosres.2017.10.023,
911   2018.

912   Nordeng, T. E. and Rasmussen, E. A. D.-:10. 1034/j. 1600-0870. 1992. 00001. x: A most
913   beautiful polar low. A case study of a polar low development in the Bear Island region, Tellus A,
914   44, 81–99, 1992.

915   Otkin, J. A. and Martin, J. E.: A synoptic climatology of the subtropical Kona storm, Mon.
916   Weather Rev., 132, 1502–1517, https://doi.org/10.1175/1520-
917   0493(2004)132<1502:ASCOTS>2.0.CO;2, 2004.

918   Parker, D. J. and Thorpe, A. J.: Conditional convective heating in a baroclinic atmosphere: a
919   model of convective frontogenesis, J. Atmospheric Sci., 52, 1699–1711,
920   https://doi.org/10.1175/1520-0469(1995)052<1699:CCHIAB>2.0.CO;2, 1995.

921   Pytharoulis, I., Craig, G. C., and Ballard, S. P.: Study of the Hurricane-like Mediterranean
922   cyclone of January 1995, Phys. Chem. Earth Part B Hydrol. Oceans Atmosphere, 24, 627–632,
923   https://doi.org/10.1016/S1464-1909(99)00056-8, 1999.

924   Romero, R. and Emanuel, K. D.-:10. 1002/jgrd. 50475: Medicane risk in a changing climate, J
925   Geophys Res, 118, 2013.

926   Rotunno, R. and Emanuel, K. A.: An air-sea interaction theory for tropical cyclones. Part II., J
927   Atmos Sci, 44, 542–561, 1987.

928   Rousseau-Rizzi, R. and Emanuel, K.: An evaluation of hurricane superintensity in axisymmetric
929   numerical models, J. Atmospheric Sci., 76, 1697–1708, https://doi.org/10.1175/jas-d-18-0238.1,
930   2019.

931   Sardie, J. M. and Warner, T. T. D.-:10. 1111/j. 1600-0870. 1985. tb00444. x: A numerical study
932   of the development mechanisms of polar lows, Tellus A, 37A, 460–477, 1985.

933   Simpson, R. H.: Evolution of the Kona storm: A subtropical cyclone, J. Atmospheric Sci., 9, 24–
934   35, https://doi.org/10.1175/1520-0469(1952)009<0024:EOTKSA>2.0.CO;2, 1952.

935 Tomita, H. and Tanaka, R.: Ocean surface warming and cooling responses and feedback
936 processes associated with polar lows over the Nordic seas, J. Geophys. Res. Atmospheres,
937 129, e2023JD040460, https://doi.org/10.1029/2023JD040460, 2024.

938 Tous, M. and Romero, R. D.-:10. 1002/joc. 3428: Meteorological environments associated with
939 medicane development, Int. J. Climatol., 33, 1–14, 2013.

940 Velez-Pardo, M. and Cronin, T. W.: Large-scale circulations and dry tropical cyclones in direct
941 numerical simulations of rotating Rayleigh-Bénard convection, J. Atmospheric Sci.,
942 https://doi.org/10.1175/JAS-D-23-0018.1, 2023.

943 Wernli, H., Dirren, S., Liniger, M. A., and Zillig, M.: Dynamical aspects of the life cycle of the
944 winter storm 'Lothar' (24–26 December 1999), Q. J. R. Meteorol. Soc., 128, 405–429,
945 https://doi.org/10.1256/003590002321042036, 2002.

946 Winschall, A., Sodemann, H., Pfahl, S., and Wernli, H.: How important is intensified evaporation
947 for Mediterranean precipitation extremes?, J. Geophys. Res. Atmospheres, 119, 5240–5256,
948 https://doi.org/10.1002/2013JD021175, 2014.

949 Yanase, W. and co-authors: Climatology of polar lows over the Sea of Japan using the JRA-55
950 reanalysis, J Clim., 29, 419–437, 2016.

951 Yarovaya, D. A., Efimov, V. V., Shokurov, M. V., Stanichnyi, S. V., and Barabanov, V. S.: A
952 quasitropical cyclone over the Black Sea: Observations and numerical simulation, Phys.
953 Oceanogr., 18, 154–167, https://doi.org/10.1007/s11110-008-9018-2, 2008.

954 Zhang, W., Villarini, G., Scoccimarro, E., and Napolitano, F.: Examining the precipitation
955 associated with medicanes in the high-resolution ERA-5 reanalysis data, Int. J. Climatol., 41,
956 E126–E132, https://doi.org/10.1002/joc.6669, 2021.

957 Zhang, Y., Meng, Z., Zhang, F., and Weng, Y.: Predictability of tropical cyclone intensity
958 evaluated through 5-yr forecasts with a convection-permitting regional-scale model in the
959 Atlantic basin, Wea Forecast., 29, 1003–1022, 2014.

960